

Title: Resource allocation by the marine cyanobacterium *Synechococcus* WH8102 in response to different nutrient supply ratios

Authors: Céline Mouginot¹, Amy E. Zimmerman^{2,a}, Juan A. Bonachela³, Helen Fredricks⁴, Steven D. Allison^{1,2}, Benjamin A. S. Van Mooy⁴, and Adam C. Martiny^{1,2*}

¹Department of Earth System Science, ²Department of Ecology and Evolutionary Biology, University of California, Irvine, California

³MASTS Marine Population Modelling Group, Department of Mathematics and Statistics, University of Strathclyde, Glasgow, United Kingdom

⁴Departments of Marine Chemistry and Geochemistry, Woods Hole Oceanographic Institution, Woods Hole, Massachusetts

*Corresponding Author

3208 Croul Hall

Irvine, California 92697

Phone: 949-824-9713

E-mail: amartiny@uci.edu

Present address:

^aMonterey Bay Aquarium Research Institute, Moss Landing, California

24

25 **Running Title:** Elemental stoichiometry of *Synechococcus*

26 **Acknowledgement:**

27 We thank Erik Lee, Agathe Talarmin, and Cecilia Batmalle Kretz for help with the
28 experiments and Don Serio for assisting us with field sampling. Financial support for this
29 work was provided by the National Science Foundation Dimensions of Biodiversity,
30 Biological Oceanography, and Major Research Instrumentation programs.

31

32

Abstract:

Differences in relative availability of nitrate vs. phosphate may contribute to regional variations in plankton elemental stoichiometry. As a representative of the globally abundant marine *Synechococcus*, strain WH8102 was grown in 16 chemostats up to 52 days at a fixed growth rate with nitrogen-phosphorus ratios ($N:P_{supply}$) of 1 to 50. Initially, the phosphate and nitrate concentrations in the vessel decreased when the respective nutrient was limiting. Cell growth generally stabilized, although several chemostats had apparent oscillations in biomass. We observed extensive plasticity in the elemental content and ratios. $N:P_{cell}$ matched the supply values between $N:P_{supply}$ 5 and 20. The $C:P_{cell}$ followed a similar trend. In contrast, the mean $C:N_{cell}$ was 6.8 and did not vary as a function of supply ratios. We also observed that induction of alkaline phosphatase, the fraction of P allocated to nucleic acids, and the lipid sulfoquinovosyldiacylglycerol:phosphatidylglycerol ratio inversely correlated with P availability. Our results suggest that this extensive plasticity in the elemental content and ratios depends both on the external nutrient availability as well as past growth history. Thus, our study provides a quantitative understanding of the regulation of the elemental stoichiometry of an abundant ocean phytoplankton lineage.

50 **Main Text:**

51 **Introduction:**

52 The elemental content of marine microbial communities is central to ocean
53 biogeochemistry as cellular nutrient requirements link the global cycles of different
54 elements (Redfield 1958). It has become apparent that the elemental composition of
55 communities is not static but rather varies between different ocean regions. This variation
56 includes elevated C:P, N:P, and C:N ratios in the high temperature but low nutrient gyres,
57 and lower ratios in high nutrient regions like upwelling zones or high latitude waters
58 (Martiny et al. 2013a; b). Such variations have a direct impact on our understanding of
59 nutrient limitation patterns and rates of nitrogen fixation (Mills and Arrigo 2010).
60 Furthermore, these regional differences in elemental stoichiometry are reflected in
61 exported particles and thus may have long-term impacts on ocean nutrient ratios (Weber
62 and Deutsch 2010; Teng et al. 2014).

63 Recent studies have demonstrated extensive differences in the elemental
64 stoichiometry of bulk particles as well as within specific phytoplankton lineages (Geider
65 and La Roche 2002; Martiny et al. 2013a; b). Part of this variation has been attributed to
66 latitudinal differences in temperature, nutrient availability, and plankton diversity.
67 Regional differences in the elemental stoichiometry between the ocean gyres have also
68 been demonstrated (Martiny et al. 2013a; b). Such variations between the gyres do not
69 appear to be linked to temperature and overall nutrient concentrations but may be due to
70 changes in the relative availability of nitrogen vs. phosphorus.

71 There are multiple theoretical models for how phytoplankton regulate cellular
72 composition in response to different environmental conditions (Droop 1973; Sterner and

Elser 2002; Klausmeier et al. 2004; Bonachela et al. 2013). Some models directly describe the cell quota (Q) of C, N, and P, whereas others derive Q from the macromolecular composition of the cell. The general concept is that nutrient and energy acquisition require N-rich proteins, growth requires P-rich ribosomes, and nutrient storage molecules may contain high N or P. According to the “growth rate hypothesis” (Sterner and Elser 2002), differences in growth rate imply differences in rRNA concentration and therefore cellular N:P ratios. Models also predict a large impact of N vs. P availability ($N:P_{supply}$) on cellular composition, whereby cells will match the $N:P_{supply}$ (Droop 1973). Alternatively, cells may be more biochemically plastic at low growth rates, but more constrained at high growth rates (Klausmeier et al. 2004) or once the cell reaches maximum or minimum physiological quotas (Bonachela et al. 2013).

The experimental support for these predictions almost exclusively comes from chemostats as such a setup allows for separation of growth vs. $N:P_{supply}$ effects. Some analyses show that N:P and C:P ratios decrease as a function of growth rate (Elrifi and Turpin 1985; Makino et al. 2003), whereas the opposite trend may occur at sufficiently low $N:P_{supply}$ (Goldman et al. 1979). There is also some evidence that phytoplankton stoichiometry can match the nutrient supply ratio (Rhee 1978; Leonardos and Geider 2004). However, unique maximum and minimum cell quotas have been found for some species, which ultimately may limit elemental ratios (Rhee 1978).

Although there are some studies of phytoplankton stoichiometry, extrapolating the results to the global ocean remains difficult due to the limited diversity of strains studied. So far, experiments have mostly focused on either large eukaryotic phytoplankton (e.g., *Dunaliella*, *Rhinomonas*, and *C. muelleri*) and/or freshwater species (e.g., *Selenastrum* or

96 *Scenedesmus*). Many of these lineages are rare or absent in the ocean and we know little
97 about how the elemental composition of the small and abundant marine cyanobacteria
98 like *Prochlorococcus* and *Synechococcus* respond to different nutrient supply ratios.

99 The minimum N and P quotas required for growth vary with cell size (Edwards et
100 al. 2012), so small phytoplankton lineages may have unique stoichiometric responses to
101 nutrient supply. We hypothesize that *Synechococcus* elemental and biochemical
102 composition would track nutrient supply ratios at intermediate values, but will deviate at
103 extreme supply ratios due to physiological constraints. To address this hypothesis, we
104 analyzed the cellular composition of *Synechococcus* strain WH8102 isolated from the
105 open ocean in response to different nutrient supply ratios. Specifically, we asked (i) what
106 is the elemental content of *Synechococcus* WH8102 when growing under different
107 nutrient supply ratios and (ii) what is the concentration of key macromolecules in the cell
108 under these different nutrient conditions? We used a chemostat approach to examine
109 $N:P_{supply}$ effects on *Synechococcus* elemental composition independent of growth rate.

111 **Methods**

112 **Culture conditions:** An axenic culture of an open ocean *Synechococcus sp.* strain
113 WH8102 (CCMP 2370) was cultured in modified SN medium at 24°C. The medium
114 differs from the regular SN medium by the nitrate and phosphate concentrations as listed
115 in Table 1. But as in SN, trace metals are buffered with citrate rather than EDTA and the
116 salinity of the natural seawater is reduced by adding 25% dH₂O (Waterbury et al. 1986).
117 Seawater collected at the San Pedro Ocean Time-series (33.3° N, 118.2° W), was filtered

at 0.22 μm , diluted to 75% with milli-Q water, and autoclaved before being enriched with nutrients and trace elements.

Air contamination is always a great concern in continuous phytoplankton culture experiment and cannot be completely eliminated. Therefore, we included multiple checks in our experimental protocols. First, the absence of heterotrophic bacteria contamination was assessed before and during experiments by checking for growth in marine LB broth (autoclaved mix of seawater, tryptone (10 g/L) and yeast extract (5 g/L) adjusted to a pH of 7.8). The presence of non-pigmented cells was also checked by flow cytometry (Accuri C6 Flow Cytometer, BD Biosciences, San Jose, California) using a blue laser and different detectors (side and light scatter - green and red fluorescence 530/30BP and 670LP). Before the reading, samples were fixed with glutaraldehyde at a final concentration of 0.1% (Polysciences, Warrington, Pennsylvania) and incubated in the dark for 15 min with 10000x diluted SybrGreen (Life Technologies, Grand Island, New York). Despite our meticulous effort to keep the system axenic, we detected instances of external contamination of heterotrophic bacteria and removed those samples from our analysis. The source of bacteria was likely air contamination or when replacing the culture medium.

Chemostat setup and parameters: Four experiments of four continuous cultures each were run for 50 days (Figure S1, www.aslo.org/lo/toc/vol_xx/issue_x/xxxxa1.pdf). Each culture included 3 polycarbonate Nalgene (Lima, Ohio) laboratory bottles: a vessel of 8 L of sterile fresh medium, 4 L of culture, and a waste reservoir. The incubator maintained a constant temperature of 24°C and was programmed for a 12:12 light-dark cycle using a

141 photon flux density of $35 \mu\text{E}/\text{m}^2/\text{s}$ during the day. On one side of the incubator were
142 placed 4 medium reservoirs and on the other side 4 culture vessels were placed on stirring
143 plates. 4 waste reservoirs were stored outside the incubator. Vessels were connected to a
144 peristaltic pump (PumpPro, Watson Marlow, Wilmington, Massachusetts) by Masterflex
145 tygon pump tubing (Cole-Parmer Vernon Hills, Illinois) and manifold Marprene long life
146 process tubing (Watson Marlow, Wilmington, Massachusetts). Pump rate varied around
147 70 rpm. Culture vessels were bubbled with an air pump (Penn-Plax Inc., Hauppauge,
148 New York). Cultures were grown at a constant dilution rate of 0.5 d^{-1} and sampled three
149 times per week into 250 ml flasks from a sampling port located just before waste
150 reservoirs.

151
152 **Cell counts:** Duplicates of 1 ml diluted samples were incubated for 15 min in the dark
153 with glutaraldehyde (final concentration 0.1%, Polysciences, Warrington, Pennsylvania)
154 and enumerated on a flow cytometer at a flow rate of $14 \mu\text{L}/\text{min}$. Cells and pigments
155 were excited at 488 nm by a blue laser and discriminated based on their orange and red
156 fluorescence using 584/40BP and 670LP filters.

157
158 **Particulate organic matter:** Particulate organic carbon (POC), nitrogen (PON) and
159 phosphorus (POP) samples were collected in duplicate by filtration of 50 ml of culture
160 onto precombusted (5 h, 500°C) GF/F filters (Whatman, Florham Park, New Jersey) and
161 stored at -20°C . To quantify POC and PON, filter samples were thawed and allowed to
162 dry overnight at 65°C . Filters were then packed into a 30 mm tin capsule (CE Elantech,
163 Lakewood, New Jersey) and analyzed for C and N content on a FlashEA 1112 nitrogen

and carbon analyzer (Thermo Scientific, Waltham, Massachusetts) (Sharp 1974). POC and PON concentrations were calibrated using known quantities of atropine and peach leaves in each run. The amount of POP was determined in each sample using a modified ash-hydrolysis method (Lomas et al. 2010).

Nutrients: 50 ml of nitrate and phosphate samples were collected by filtration through a 0.2 μm syringe filter and stored at -20°C . Dissolved inorganic phosphate concentrations were determined using the MAGIC-SRP method and calculated against a potassium monobasic phosphate standard (Lomas et al. 2010). Nitrate samples were treated with ethylenediamine-tetraacetate solution and passed through a column of copperized cadmium filings according to the Bermuda Atlantic Time-Series study methods (<http://bats.bios.edu/methods/chapter9.pdf>). Detection limits of nitrate and phosphate measurements were respectively 80 and 40 nmol L^{-1} .

Nucleic acid content: DNA and RNA were quantified as previously described (Zimmerman et al. 2014a). In brief, replicate 50 ml samples from each vessel were collected on precombusted (5 h, 500°C) GF/F filters (Whatman, Florham Park, New Jersey). Filters were placed into a bead beater tube with 0.65 g of 0.1 mm glass beads (MO BIO Laboratories Inc., Carlsbad, California), flash frozen in liquid nitrogen, and stored at -80°C until analysis. Nucleic acids were released from filters by mechanical lysis (MP FastPrep-24 bead beater, MP Biomedicals, Solon, Ohio) in a mix of 800 μL of Tris buffer (5 mmol L^{-1}) and 200 μL of RNA preservative (saturated ammonium sulfate solution). Sample supernatant was used to prepare assays in 96-well microplates with the

Qubit dsDNA or RNA HS Assay kits (Life technologies, Eugene, Oregon). Fluorescence was measured on a SpectraMax M2 microplate reader (Molecular Devices, Sunnyvale, California). The fraction of P in each nucleic acid was estimated based on the average molecular weight of a nucleotide in DNA and RNA (340 and 330 g/mol, respectively).

Enzyme activity: To characterize the impact of different $N:P_{supply}$ on alkaline phosphatase activity, potential enzyme activity was quantified for each chemostat (Allison et al. 2012). Briefly, 50 μ L of varying concentrations (2-200 μ mol L⁻¹) of fluorometric substrate (4-methyl-umbelliferyl phosphate, Sigma-Aldrich) were combined with 200 μ L of fresh culture sample in a black 96-well microplate (Greiner Bio-One) and incubated for 1 hour at room temperature. During the incubation, the microplates were measured at 360 nm excitation/460 nm emission in a fluorometer (BioTek Synergy 4) at 0, 15, 30, 45, and 60 minutes. Sample blanks (200 μ L culture + 50 μ L DI water) were included to account for the background fluorescence of each sample, and substrate blanks (200 μ L un-inoculated media + 50 μ L substrate solution) were included to account for autohydrolysis of the substrate during the assay incubation. To determine conversion of fluorescence to product concentration and to account for quenching of fluorescence by the sample, 50 μ L of standard solution (4-methyl-umbelliferone, Sigma-Aldrich) was added at a final concentration of 10 μ mol L⁻¹ to sample or uninoculated media.

The concentration of reaction product in the sample wells was determined based on the standard, after correcting for the substrate blank and sample blank described. The fluorescence values used for samples and substrate blanks represent the means of 3 or 4 replicate wells, while the values used for the standard and sample blanks represent the

means of 8 replicate wells. Enzyme activity values that showed substrate inhibition at high substrate concentrations were dropped prior to the regression analysis, and V_{max} and standard error values were estimated by fitting a hyperbolic curve to the resulting activities.

Lipids: To determine the lipid composition of the cells, 3 replicates of 150 mL culture were filtered on precombusted (5 h, 500°C) GF/F filters (Whatman, Florham Park, New Jersey) and analyzed for three classes of glycolipids (monoglycosyldiacylglycerol, MGDG, diglycosyldiacylglycerol, DGDG and sulfoquinovosyldiacylglycerol, SQDG), three classes of phospholipids (phosphatidylglycerol, PG, phosphatidylethanolamine, PE and phosphatidylcholine, PC), and three classes of betaine lipids (diacylglyceryl trimethylhomoserine, DGTS, diacylglyceryl hydroxymethyl-trimethyl- β -alanine, DGTA and diacylglyceryl carboxyhydroxymethylcholine, DGCC). Lipids were analyzed using high performance liquid chromatography/electrospray-ionization triple-quadrupole mass spectrometry (HPLC-ESI-TQMS) with a Hewlett Packard 1200 HPLC instrument and Thermo TSQ Vantage mass spectrometer (Pependorf et al. 2013). The canonical cyanobacterial lipids are MGDG, DGDG, SQDG, and PG (Wada and Murata 1998), but other lipids were monitored nonetheless to assess the presence of heterotrophic bacteria. Samples with a high concentration of non-cyanobacterial lipids were those presented as contaminated after axenic test in LB broth and control by flow cytometry and, were subsequently eliminated from the analysis.

Results:

233 In order to identify the cellular response to different nutrient conditions, we grew
 234 *Synechococcus* WH8102 in chemostats with a dilution rate of 0.5 d^{-1} at 16 different
 235 nutrient supply ratios ($N:P_{\text{supply}}$) ranging from 1 to 50 (Table 1). We monitored cell
 236 abundances, dissolved nutrient concentrations, and cellular nutrient quotas (and ratios) up
 237 to 52 days for all 16 chemostats (Figure S1). For chemostats with lower $N:P_{\text{supply}}$, the
 238 nitrate concentration (i.e., $\text{nitrate}_{\text{vessel}}$) dropped during the first 10 days as cells nearly
 239 exhausted the N source (Figure S2). However, $\text{nitrate}_{\text{vessel}}$ rarely reached detection limits.
 240 In contrast to $\text{nitrate}_{\text{vessel}}$, $\text{phosphate}_{\text{vessel}}$ was high at very low $N:P_{\text{supply}}$. At $N:P_{\text{supply}} \geq 10$,
 241 *Synechococcus* WH8102 was capable of taking up all the available phosphate and
 242 $\text{phosphate}_{\text{vessel}}$ dropped below the detection limit. On average, the chemostats supported \sim
 243 10^{10} cells/L and cell abundances largely followed the same temporal trend in all
 244 chemostats. Specifically, cell numbers increased initially until N and/or P was low in the
 245 chemostat and then dropped. In some chemostats ($N:P_{\text{supply}} = 5, 7, 10, 12, 15, 22, 35$, and
 246 38), cell abundances appeared to reach an equilibrium. In other chemostats, we observed
 247 that cell abundances declined following the exhaustion of nutrients. This decline led to
 248 oscillations with no apparent steady-state biomass concentration (e.g., $N:P_{\text{supply}} = 20$) for
 249 the duration of the chemostat run.

250 The concentrations of total cellular carbon and nitrogen (i.e., POC and PON)
 251 followed a similar temporal trend as cell abundances (Figure S2). POC and PON
 252 increased initially and then stabilized at concentrations of $200 - 600 \mu\text{mol C L}^{-1}$ and $20 -$
 253 $80 \mu\text{mol N L}^{-1}$, respectively. Thus, POC and PON did not vary as strongly temporally as
 254 the cell abundances. In contrast, the temporal variability in POP did not always match
 255 POC and PON and especially at high $N:P_{\text{supply}}$, all inorganic P was incorporated into

cellular biomass. We also examined the cell quota (Q) and found large temporal intra-chemostat variations. For example, Q_C tripled over a ten-day period in the chemostat with $N:P_{supply} = 5$. The same was observed for Q_N and Q_P . Such temporal changes in Q were observed across all chemostats. We also compared Q_C to the flow cytometry forward scatter and observed that these two independent assessments of cell size were highly correlated ($r_{spearman} = 0.74$, $p < 1 \times 10^{-7}$) and showed very similar temporal trends (Fig. S3). The increase in cell size and biomass was related to growth physiology, whereby cells were larger during periods of high nutrient availability and just prior to increases in cell abundances. We examined cellular elemental ratios and found limited differences in $C:N_{cell}$, whereas $N:P_{cell}$ and $C:P_{cell}$ typically increased initially and then dropped once nutrients in the chemostat were exhausted.

Despite some temporal variability across chemostats, we quantified the mean cell quotas and elemental ratios across the last 20 days of each chemostat (Figure 1). The mean cell quotas across all $N:P_{supply}$ were 211 fg C, 36 fg N, and 6 fg P (Figure 1 A-C and Table 1). Across chemostats with different $N:P_{supply}$, Q_P decreased non significantly while Q_N and Q_C did not. This was in part due to considerable temporal and between-chemostat variations in cell size. The mean $C:N_{cell}$ was 6.8 and thus close to Redfield proportions (Figure 1D). Further, this ratio did not vary significantly across different $N:P_{supply}$. In contrast, we saw significant responses for both $C:P_{cell}$ and $N:P_{cell}$ (Figure 1E and F). $C:P_{cell}$ increased from 50 to 180 for $N:P_{supply}$ 1 to 22. At higher $N:P_{supply}$, there was little change in the $C:P_{cell}$. With a similar shape, $N:P_{cell}$ ranged from 5 to 30 and thus largely matched the $N:P_{supply}$ at lower ratios and then stabilized at high $N:P_{supply}$.

We examined the impact of different $N:P_{supply}$ on the expression of alkaline phosphatase, nucleic acid content, and lipid profiles (Figure 2). The alkaline phosphatase expression for each chemostat was quantified using fluorometric substrates and reported as the maximum reaction velocity (V_{max}). For alkaline phosphatase, we found a significant positive induction of enzyme activity in relation to increasing $N:P_{supply}$ (Figure 2A). At $N:P_{supply} \leq 10$, V_{max} was close to detection limits. Above this supply level, V_{max} rose steadily as a function of $N:P_{supply}$ and reached a maximum at $N:P_{supply} = 42$. V_{max} was also linked to $N:P_{cell}$ ($r_{spearman} = 0.629$, $p = 0.0116$) suggesting that internal nutrient requirements could contribute to the level of phosphatase expression. Thus, the degree of P limitation (and change in $N:P_{cell}$) had a quantitative effect on enzyme V_{max} .

The mean concentrations of DNA and RNA were 3.7 and 3.9 fg/cell, respectively, and each nucleic acid contributed on average 9% of total cellular P (Table 1). The fraction of cellular P in nucleic acids varied between 2 and 27%, and this fraction increased significantly with $N:P_{supply}$ (Fig. 2B). In contrast (data not shown), we did not observe a significant relationship between the absolute level of nucleic acids and $N:P_{supply}$.

Finally, we quantified the lipid content of *Synechococcus* WH8102 across chemostats and found that phosphorus stored in lipids accounted for on average 4 % (1.1 – 9) of Q_P (Table 1). We then examined the ratio of sulfo- to phospholipids (SQDG:PG) as this has been demonstrated to change with P stress (Van Mooy et al. 2009) (Figure 2C). We observed a clear correlation between Q_P whereby cells with a low Q_P had a high SQDG:PG. However, the lipid ratio was not only linked to $N:P_{supply}$. For example, the ratio was 33.2 on week 4 and 9.6 on week 5 in a chemostat with a constant $N:P_{supply}$ of

35. Thus, it appeared that a combination of past growth history and nutrient availability affected the lipid content.

Discussion:

Consistent with our initial hypothesis, we found that the elemental stoichiometry of a cultured representative of *Synechococcus* – a very abundant phytoplankton in the ocean (Flombaum et al. 2013) – changes as a function of $N:P_{supply}$. Flexibility in elemental composition is consistent with past studies of phytoplankton (Rhee 1978). In addition, our work suggests lower and upper limits of elemental ratios, specifically in *Synechococcus*. Limits are especially clear at high $N:P_{supply}$ ratios, where cell stoichiometry approximates a constant value (Fig. 1). This plateau is mostly driven by the phosphorus quota, Q_P , which reaches a minimum. Thus, our data supports a physiological limit constraining cellular stoichiometry and resource allocation strategies (Pahlow and Oschlies 2009; Bonachela et al. 2013). It is worth noting that there is extensive genomic diversity within marine *Synechococcus* that can influence nutrient uptake, growth physiology, and ultimately their C:N:P ratios (Scanlan et al. 2009). Furthermore, strain WH8102 was isolated more than 30 years ago and may have undergone some genetic change in the laboratory. However, in a recent comparison of two *Synechococcus* strains, little variability was detected suggesting that our results are generally applicable to this genus (Kretz et al. 2015).

Studies with a single nutrient have shown a link between external nutrient concentration and nutrient-uptake protein expression (Tetu et al. 2009). However, the linked response of alkaline phosphatase expression to $N:P_{supply}$ and $N:P_{cell}$ supports a

regulation of biochemical allocation to nutrient acquisition (Fig. 2A), whereby N and P may interact at the cellular level and determine the protein expression. Such an interaction is consistent with results for nitrogen-related V_{max} using various growth rates and supply ratios (Rhee 1978), and indicates that internal nutrient requirements influence the expression of nutrient-acquiring enzymes (Bonachela et al. 2013). More specifically, in cases of high levels of cellular N, low P content in the cell allows phytoplankton to up-regulate the synthesis of nutrient-uptake proteins, thereby increasing the uptake rate of such nutrient. Conversely, high levels of P allow the cell to down-regulate P-uptake protein synthesis and allocate those resources to other cellular functions.

We found that between 5 and 30% of cellular P is tied up in nucleic acids and between 1 and 9 % in polar lipids. These fractions are consistent with other recent studies of marine microorganisms and communities (Van Mooy et al. 2006; Zimmerman et al. 2014a; b) and show that the majority of P is present in other cellular fractions. These may include storage compounds such as poly-phosphate (Martin et al. 2014). We also observed that with increasing $N:P_{supply}$, nucleic acids constitute an increasing fraction of cellular P (Fig. 2B) but with no trend in absolute concentrations. Again, this result is consistent with field observations (Zimmerman et al. 2014b) and suggests that absolute nucleic acid concentrations may be more strongly tied to growth rate than the availability of a specific nutrient. Our observations and previous studies also suggest that other P fractions may be declining as a function of P availability. The distribution of the data also confirm that a subset of cultures can have lower SQDG:PG lipid ratios in cells with low Q_P . The exact mechanism for this is unclear but it is consistent with past observations of variability at low Q_P in lipid content of *Synechococcus* (Van Mooy et al. 2006). Thus,

Synechococcus WH8102 generally responds to declining P availability by increasing enzyme mediated nutrient acquisition as well as reducing allocations to lipids and unknown P pools, although there appear to be complex dynamics at play when Q_P is at its lowest extreme.

Synechococcus WH8102 cell quotas quantified in this study are within the bounds of previous observations but also suggest extensive plasticity. In a past analysis of the elemental content of *Synechococcus* strains, Bertilsson et al. (2003) detected cell quotas of 92 to 244 fg C, 20 to 50 fg N, and 0.47 to 3.34 fg P. Similarly, Heldal et al. (2003) found cell quotas of 120 to 250 fg C, 17 to 36 fg N, and 2.6 to 7.9 fg P. We also observed a three-fold variation in the cellular carbon content, a result confirmed independently by flow cytometry. The mechanisms controlling this change in biomass are unknown but may be related to nutrient availability and growth physiology as has been seen in other organisms (Schaechter et al. 1958). It appears that cells are largest during periods of increasing cell abundances and thus when the population growth rate is higher than the dilution rate.

We found strong temporal differences in both cell abundances and carbon cell quotas of *Synechococcus* WH8102, and not all chemostats reached a clear steady-state. Part of the temporal variation appears to be related to nutrient concentrations, whereby cell abundances drop following the exhaustion of nutrients (Figure S2). This may be due to an extensive time-lag in physiological acclimation to low nutrient conditions as previously seen in both *Prochlorococcus* and *Synechococcus* (Martiny et al. 2006; Tetu et al. 2009). Theoretical models also predict that such a response time-lag can cause oscillations in biomass and not lead to a single equilibrium value (Xia et al. 2005).

Unstable population densities have also been observed for other species (Caperon 1969). Overall, this result suggests that the physiological history of the cell can have a large impact on the observed elemental content and ratio and thus partly obscure the link between environmental conditions and cellular content.

We examined the cell physiology of *Synechococcus* in response to differences in the relative availability of N vs. P. By using a chemostat setup, we further isolated the effect of nutrient supply ratios without a confounding effect of changes in average growth rate. We found extensive plasticity in the N or P cell quotas that make it difficult to interpret the absolute cell quotas in relation to nutrient availability. This variation appears to be caused by significant changes in overall cell size and biomass driven by the past growth history. Similarly, the levels of nucleic acids showed considerable variability that are likely linked to these putative cell size changes and possibly growth history. In contrast, lipid profiles, alkaline phosphatase induction, and cellular nutrient ratios are excellent biomarkers for nutrient stress. Furthermore, our study identifies novel controls on elemental stoichiometry and biochemical allocation in relation to the relative availability of N and P. Considering the large contribution of marine cyanobacteria to ocean primary production (Flombaum et al. 2013), such information can be important for understanding the role of nutrient availability in controlling the elemental stoichiometry of ocean communities and their contribution to productivity.

References:

Allison, S. D., Y. Chao, J. D. Farrara, S. Hatosy, and A. C. Martiny. 2012. Fine-scale temporal variation in marine extracellular enzymes of coastal southern California. *Front. Microbiol.* **3**, doi:10.3389/fmicb.2012.00301

- 394 Bonachela, J. A., S. D. Allison, A. C. Martiny, and S. A. Levin. 2013. A model for
395 variable phytoplankton stoichiometry based on cell protein regulation.
396 Biogeosciences **10**: 4341–4356.
- 397 Caperon, J. 1969. Time lag in population growth response of *Isochrysis galbana* to a
398 variable nitrate environment. Ecology **50**: 188–192.
- 399 Droop, M. R. 1973. Some thoughts on nutrient limitation in algae. J. Phycol. **9**: 264–272.
- 400 Edwards, K., M. Thomas, C. A. Klausmeier, and E. Litchman. 2012. Allometric scaling
401 and taxonomic variation in nutrient utilization traits and maximum growth rate of
402 phytoplankton. Limnol. Oceanogr. **57**: 554–566.
- 403 Elrifi, I. R., and D. H. Turpin. 1985. Steady-state luxury consumption and the concept of
404 optimum nutrient ratios - a study with phosphate and nitrate limited *Selenastrum*
405 *minutum* (Chlorophyta). J. Phycol. **21**: 592–602.
- 406 Flombaum, P., J. L. Gallegos, R. A. Gordillo, J. Rincon, L. L. Zabala, N. Jiao, D. M.
407 Karl, W. K. W. Li, M. W. Lomas, D. Veneziano, C. S. Vera, J. A. Vrugt, and A. C.
408 Martiny. 2013. Present and future global distributions of the marine Cyanobacteria
409 *Prochlorococcus* and *Synechococcus*. Proc. Natl. Acad. Sci. U. S. A. **110**: 9824–
410 9829.
- 411 Geider, R. J., and J. La Roche. 2002. Redfield revisited: variability of C : N : P in marine
412 microalgae and its biochemical basis. Eur. J. Phycol. **37**: 1–17.
- 413 Goldman, J. C., J. J. McCarthy, and D. G. Peavey. 1979. Growth-Rate Influence on the
414 Chemical Composition of Phytoplankton in Oceanic Waters. Nature **279**: 210–215.
- 415 Klausmeier, C. A., E. Litchman, and S. A. Levin. 2004. Phytoplankton growth and
416 stoichiometry under multiple nutrient limitation. Limnol. Oceanogr. **49**: 1463–1470.
- 417 Kretz, C. B., D. W. Bell, D. A. Lomas, M. W. Lomas, and A. Martiny. 2015. Influence of
418 growth rate on the physiological response of marine *Synechococcus* to phosphate
419 limitation. Front. Microbiol. **6**, doi:10.3389/fmicb.2015.00085
- 420 Leonardos, N., and R. J. Geider. 2004. Responses of elemental and biochemical
421 composition of *Chaetoceros muelleri* to growth under varying light and nitrate:
422 phosphate supply ratios and their influence on critical N : P. Limnol. Oceanogr. **49**:
423 2105–2114.
- 424 Lomas, M. W., A. L. Burke, D. A. Lomas, D. W. Bell, C. Shen, S. T. Dyhrman, and J. W.
425 Ammerman. 2010. Sargasso Sea phosphorus biogeochemistry: an important role for
426 dissolved organic phosphorus (DOP). Biogeosciences **7**: 695–710.

- 427 Makino, W., J. B. Cotner, R. W. Sterner, and J. J. Elser. 2003. Are bacteria more like
428 plants or animals? Growth rate and resource dependence of bacterial C : N : P
429 stoichiometry. *Funct. Ecol.* **17**: 121–130.
- 430 Martin, P., S. T. Dyhrman, M. W. Lomas, N. J. Poulton, and B. a S. Van Mooy. 2014.
431 Accumulation and enhanced cycling of polyphosphate by Sargasso Sea plankton in
432 response to low phosphorus. *Proc. Natl. Acad. Sci. U. S. A.* **111**: 8089–94.
- 433 Martiny, A. C., M. L. Coleman, and S. W. Chisholm. 2006. Phosphate acquisition genes
434 in *Prochlorococcus* ecotypes: Evidence for genome-wide adaptation. *Proc. Natl.*
435 *Acad. Sci. U. S. A.* **103**: 12552–12557.
- 436 Martiny, A. C., C. T. A. Pham, F. W. Primeau, J. A. Vrugt, J. K. Moore, S. A. Levin, and
437 M. W. Lomas. 2013a. Strong latitudinal patterns in the elemental ratios of marine
438 plankton and organic matter. *Nat. Geosci.* **6**: 279–283.
- 439 Martiny, A. C., J. A. Vrugt, F. W. Primeau, and M. W. Lomas. 2013b. Regional variation
440 in the particulate organic carbon to nitrogen ratio in the surface ocean. *Global*
441 *Biogeochem. Cycles* **27**: 723–731.
- 442 Mills, M. M., and K. R. Arrigo. 2010. Magnitude of oceanic nitrogen fixation influenced
443 by the nutrient uptake ratio of phytoplankton. *Nat. Geosci.* **3**: 412–416.
- 444 Van Mooy, B. A. S., H. F. Fredricks, B. E. Pedler, S. T. Dyhrman, D. M. Karl, M.
445 Koblizek, M. W. Lomas, T. J. Mincer, L. R. Moore, T. Moutin, M. S. Rappe, and E.
446 A. Webb. 2009. Phytoplankton in the ocean use non-phosphorus lipids in response
447 to phosphorus scarcity. *Nature* **458**: 69–72.
- 448 Van Mooy, B. A. S., G. Rocap, H. F. Fredricks, C. T. Evans, and A. H. Devol. 2006.
449 Sulfolipids dramatically decrease phosphorus demand by picocyanobacteria in
450 oligotrophic marine environments. *Proc. Natl. Acad. Sci. U. S. A.* **103**: 8607–8612.
- 451 Pahlow, M., and A. Oschlies. 2009. Chain model of phytoplankton P, N and light
452 colimitation. *Mar. Ecol. Prog. Ser.* **376**: 69–83.
- 453 Popen Dorf, K. J., H. F. Fredricks, and B. A. S. Van Mooy. 2013. Molecular ion-
454 independent quantification of polar glycerolipid classes in marine plankton using
455 triple quadrupole MS. *Lipids* **48**: 185–195.
- 456 Redfield, A. C. 1958. The biological control of the chemical factors in the environment.
457 *Am. Sci.* **46**: 1–18.
- 458 Rhee, G. Y. 1978. Effects of N-P atomic ratios and nitrate limitation on algal growth, cell
459 composition, and nitrate uptake. *Limnol. Oceanogr.* **23**: 10–25.

- Scanlan, D. J., M. Ostrowski, S. Mazard, A. Dufresne, L. Garczarek, W. R. Hess, A. F. Post, M. Hagemann, I. Paulsen, and F. Partensky. 2009. Ecological genomics of marine picocyanobacteria. *Microbiol. Mol. Biol. Rev.* **73**: 249–299.
- Schaechter, M., O. Maaloe, and N. O. Kjeldgaard. 1958. Dependency on medium and temperature of cell size and chemical composition during balanced grown of *Salmonella typhimurium*. *J. Gen. Microbiol.* **19**: 592–606.
- Sharp, J. H. 1974. Improved analysis for “particulate” organic carbon and nitrogen from seawater. *Limnol. Oceanogr.* **19**: 984–989.
- Sterner, R. W., and J. J. Elser. 2002. Ecological stoichiometry: the biology of elements from molecules to the biosphere, Princeton University Press.
- Teng, Y.-C., F. W. Primeau, J. K. Moore, M. W. Lomas, and A. C. Martiny. 2014. Global-scale variations in the carbon to phosphorous ratio of exported marine organic matter. *Nat. Geosci.* **7**: 895–898.
- Tetu, S. G., B. Brahamsha, D. A. Johnson, V. Tai, K. Phillippy, B. Palenik, and I. T. Paulsen. 2009. Microarray analysis of phosphate regulation in the marine cyanobacterium *Synechococcus* sp WH8102. *ISME J.* **3**: 835–849.
- Wada, H., and N. Murata. 1998. Membrane Lipids in Cyanobacteria, p. 65–81. *In* Lipids in Photosynthesis: Structure, Function and Genetics.
- Waterbury, J. B., S. W. Watson, F. W. Valois, and D. G. Franks. 1986. Biological and ecological characterization of the marine unicellular cyanobacterium *Synechococcus*, p. 20–71. *In* T. Platt and W.K.W. Li [eds.], *Photosynthetic Picoplankton*. Department of Fisheries and Oceans.
- Weber, T. S., and C. Deutsch. 2010. Ocean nutrient ratios governed by plankton biogeography. *Nature* **467**: 550–554.
- Xia, H., G. S. K. Wolkowicz, and L. Wang. 2005. Transient oscillations induced by delayed growth response in the chemostat. *J. Math. Biol.* **50**: 489–530.
- Zimmerman, A. E., S. D. Allison, and A. C. Martiny. 2014a. Phylogenetic constraints on elemental stoichiometry and resource allocation in heterotrophic marine bacteria. *Environ. Microbiol.* **16**: 1398–1410.
- Zimmerman, A. E., A. C. Martiny, M. W. Lomas, and S. D. Allison. 2014b. Phosphate supply explains variation in nucleic acid allocation but not C : P stoichiometry in the western North Atlantic. *Biogeosciences* **11**: 1599–1611.

Table 1: Mean (and standard deviation) of chemostat variables based on the last 20 days of operation.

<i>N:P_{supply}</i>	<i>P_{supply}</i> (μ M)	<i>N_{supply}</i>	<i>Q_C</i>	<i>Q_N</i> (fg/cell)	<i>Q_P</i>	[cells] (10 ¹⁰ cells/L)	C:N	C:P (mol/mol)	N:P	DNA (fg/cell)	RNA (fg/cell)	<i>V_{max}</i> (amol/h/cell)	lipids SQDG/PG	%P _{lipid}
1	40	40	103 ₍₁₃₎	20 ₍₃₎	6.9 _(4.9)	4.5 _(1.1)	6.0 _(0.5)	51 ₍₂₅₎	8.8 _(4.7)	2.5 _(0.3)	3.0 _(0.04)	4 _(0.1)	10 ₍₁₎	
3	13.3	40	237 ₍₅₀₎	40 ₍₉₎	14 _(3.8)	2.2 _(0.8)	7.0 _(0.7)	44 ₍₅₎	6.4 _(0.5)	3.1 _(0.02)	3.6 _(0.3)	13 _(0.3)	8 ₍₁₎	1.1 _(0.1)
5	8.0	40	460 ₍₂₄₉₎	83 ₍₄₀₎	18 _(9.9)	0.7 _(0.8)	6.3 _(0.7)	68 ₍₁₃₎	11 _(3.1)	6.4 _(0.3)	8.9 _(0.2)	18 ₍₅₎		
7	5.7	40	163 ₍₃₃₎	27 ₍₆₎	5.4 _(1.4)	3.4 _(0.7)	7.1 _(0.4)	80 ₍₉₎	11 _(1.1)	3.7 _(0.1)	4.0 _(0.1)	9 ₍₁₎	27 ₍₆₎	2.2 _(0.7)
10	4.0	40	181 ₍₅₂₎	32 ₍₉₎	4.0 _(1.6)	2.5 _(0.5)	6.2 _(0.7)	113 ₍₁₉₎	19 _(4.2)	3.1 _(0.1)	4.9 _(0.3)	13 ₍₁₎	17 ₍₄₎	3.8 _(0.4)
12	3.3	40	146 ₍₂₃₎	25 ₍₅₎	3.7 _(1.1)	3.0 _(0.8)	7.0 _(0.9)	103 ₍₁₄₎	15 _(1.8)	3.3 _(0.4)	2.7 _(0.2)	117 ₍₁₅₎	40 ₍₃₎	3.0 _(0.9)
15	2.7	40	269 ₍₈₃₎	43 ₍₁₅₎	7.0 _(3.2)	2.3 _(0.9)	7.4 _(0.9)	107 ₍₂₁₎	15 _(2.6)	2.6 _(0.1)	2.4 _(0.2)		15 ₍₂₎	4.7 _(0.2)
18	2.2	40	313 ₍₂₅₁₎	46 ₍₄₁₎	4.1 _(9.5)	1.3 _(0.5)	8.2 _(1.2)	126 ₍₂₈₎	20 _(4.5)	6.7 _(0.4)	7.1 _(1.0)	23 ₍₁₎	46 ₍₈₎	2.5 _(0.6)
20	2.0	40	170 ₍₃₇₎	30 ₍₇₎	2.2 _(0.9)	2.5 _(0.5)	6.1 _(0.5)	146 ₍₁₅₎	24 _(1.7)	3.1 _(0.2)	4.1 _(0.8)	95 ₍₈₎	14 ₍₁₎	9.0 _(1.9)
22	2.0	44	107 ₍₂₉₎	18 ₍₆₎	1.7 _(0.9)	3.8 _(2.3)	6.9 _(0.4)	190 ₍₅₉₎	27 _(7.5)	2.0 _(0.04)	2.1 _(0.3)	407 ₍₃₆₎	11 ₍₁₎	
28	2.0	56	305 ₍₁₀₂₎	51 ₍₂₃₎	9.2 _(4.4)	0.7 _(0.1)	7.1 _(1.1)	92 ₍₁₃₎	13 _(2.3)	7.2 _(0.8)	4.6 _(0.6)	443 ₍₃₁₎	9 ₍₁₎	2.6 _(0.4)
30	2.0	60	104 ₍₂₇₎	18 ₍₄₎	1.9 _(0.8)	3.8 _(1.0)	6.5 _(0.3)	161 ₍₄₇₎	25 _(7.3)	2.6 _(0.7)	3.2 _(0.9)	863 ₍₂₁₉₎		
35	2.0	70	214 ₍₆₈₎	32 ₍₁₅₎	5.3 _(3.0)	1.3 _(1.0)	8.4 _(1.2)	123 ₍₄₃₎	15 _(3.5)	3.1 _(0.4)	1.7 _(1.2)	346 ₍₂₃₎		4.9 _(0.9)
38	2.0	76	148 ₍₆₉₎	27 ₍₁₂₎	3.2 _(2.1)	3.4 _(1.6)	6.5 _(0.7)	144 ₍₄₉₎	22 _(7.4)	3.6 _(0.4)	3.3 _(0.3)	922 ₍₁₈₀₎		
42	2.0	84	268 ₍₁₁₉₎	48 ₍₂₄₎	5.6 _(2.8)	1.3 _(0.5)	6.4 _(0.6)	129 ₍₂₁₎	20 _(3.5)	4.1 _(0.1)	4.3 _(0.3)	1020 ₍₁₀₂₎		6.6 _(0.6)
50	2.0	100	184 ₍₈₆₎	36 ₍₁₃₎	2.9 _(1.6)	1.8 _(1.3)	6.0 _(0.5)	173 ₍₃₀₎	29 _(6.0)	2.3 _(0.29)	1.9 _(0.5)	240 ₍₂₀₎	13 ₍₂₎	5.6 _(1.5)
Mean			211 ₍₉₅₎	36 ₍₁₆₎	6.0 _(4.5)	2.4 _(1.2)	6.8 _(0.7)	116 ₍₄₂₎	18 _(4.7)	3.7 _(1.6)	3.9 _(1.9)	525 ₍₃₆₁₎	12 ₍₁₃₎	4.2 _(2.3)

Figure Legends:

Figure 1. Mean cellular nutrient contents and ratios across 16 chemostats with different N:P nutrient supply ratios. (A) Carbon cell quota (Q_C), (B) nitrogen cell quota (Q_N), and (C) phosphorus cell quota (Q_P). Molar ratios of (D) carbon to nitrogen, (E) carbon to phosphorus, and (F) nitrogen to phosphorus. A 1:1 line is added to Fig. 1F to guide a comparison between $N:P_{supply}$ and $N:P_{cell}$. The inserted statistics represent Spearman correlations between the variables. The error bars represent one standard deviation and are based on measurements for the last 20 days of operation of each chemostat.

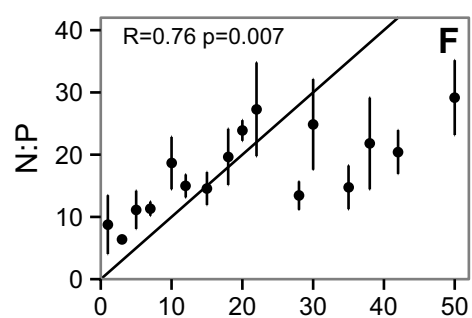
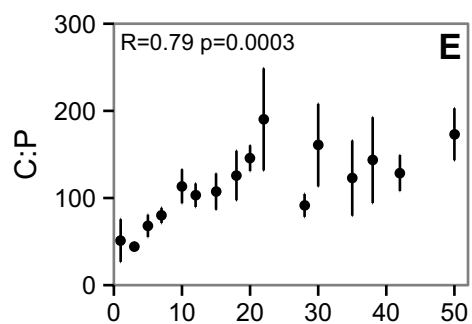
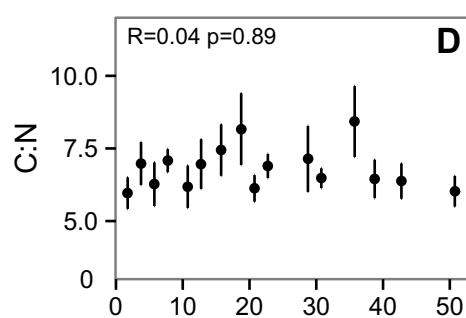
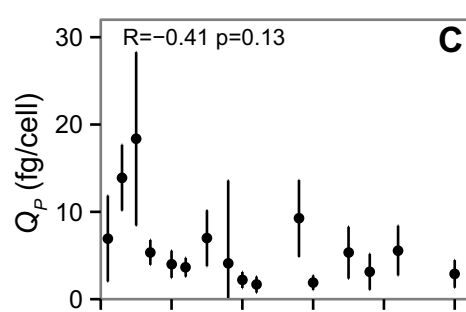
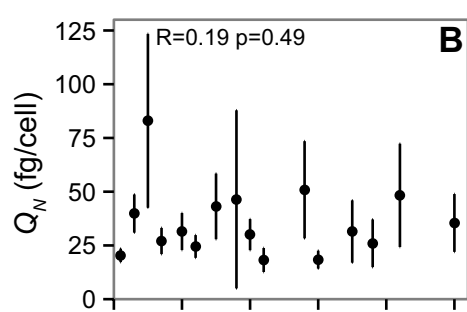
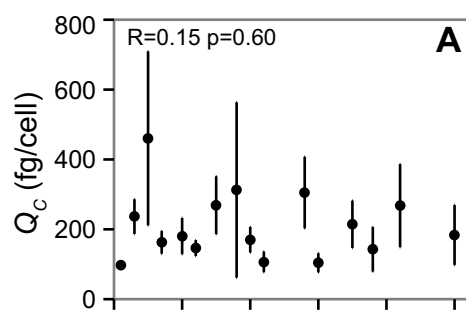
Figure 2. Mean cellular macromolecule content across 16 chemostats with different $N:P_{supply}$. (A) Alkaline phosphatase maximum activity (V_{max}) plotted with the residual phosphate concentration ($phosphate_{vessel}$). (B) Fraction of P allocated to the nucleic acids DNA and RNA. (C) Molar ratio of sulfoquinovosyldiacylglycerol (SQDG) to phosphatidylglycerol (PG) lipids as a function of the P cell quota (Q_P). The inserted statistics represent Spearman correlations between the variables.

Supplementary Information:

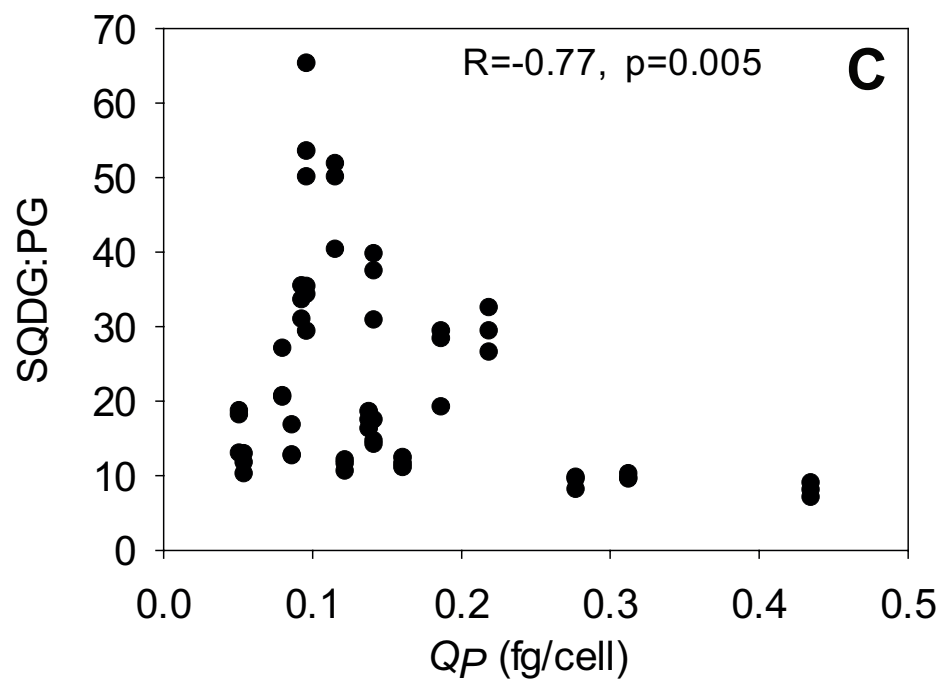
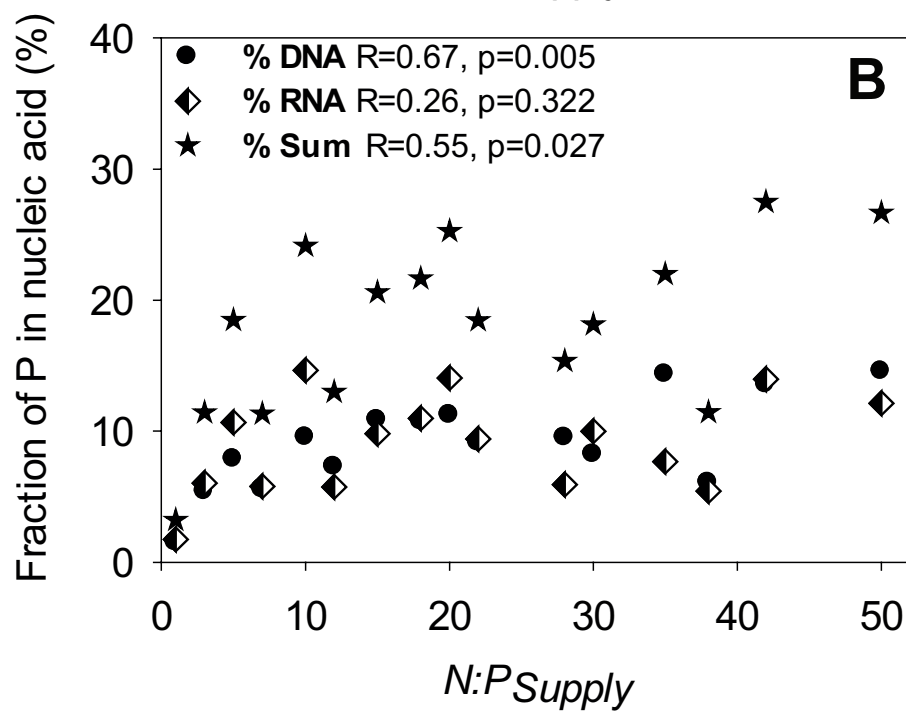
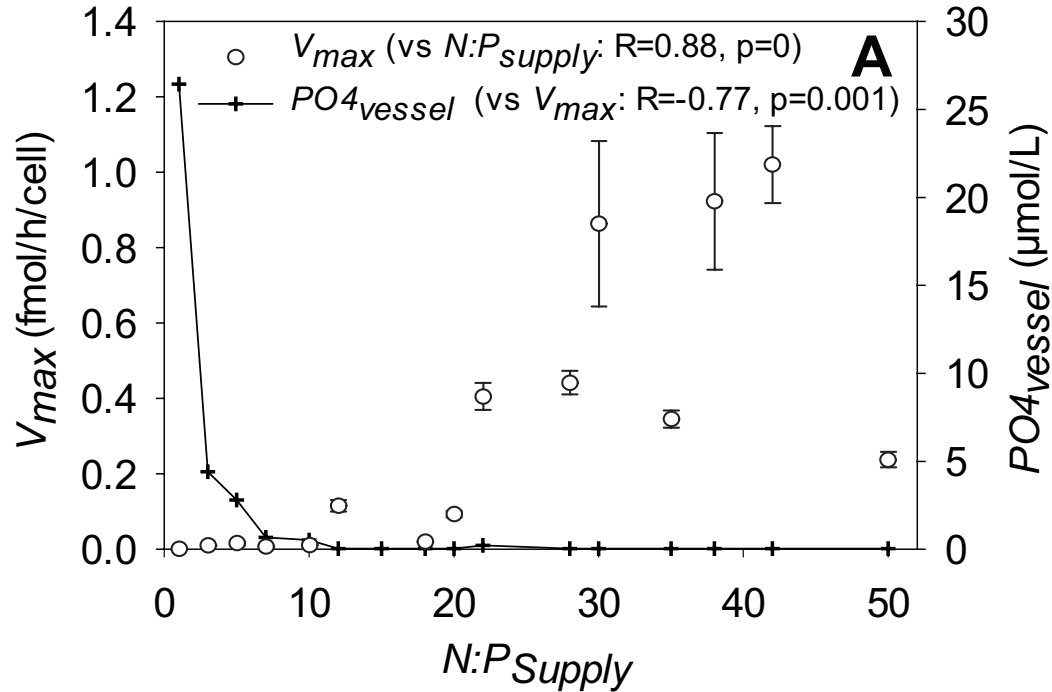
Figure S1. Overview of chemostat design.

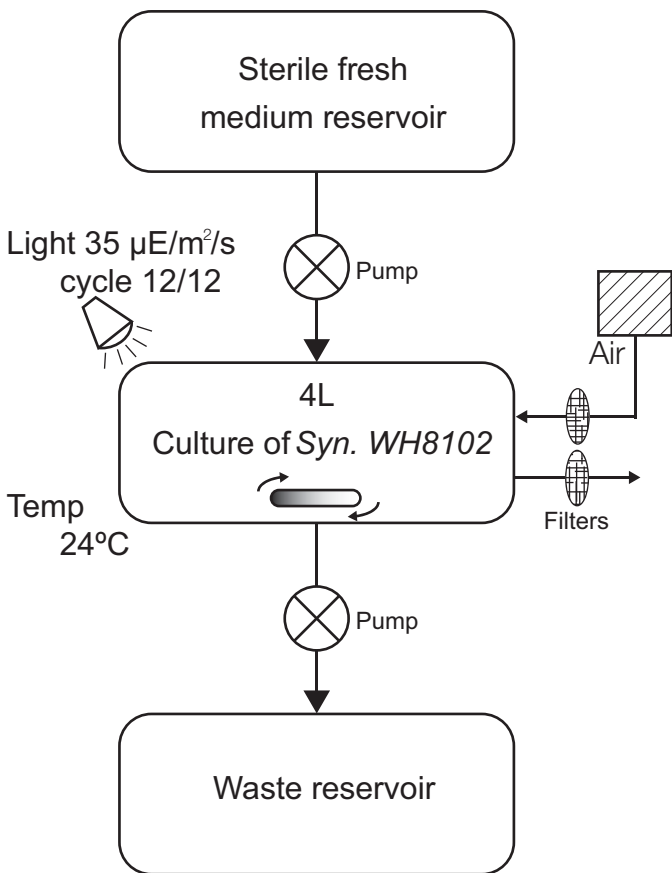
Figure S2. Temporal changes in cell and nutrient concentrations in all 16 chemostats with different nutrient supply ratios. This includes cell abundance, residual nitrate ($nitrate_{vessel}$) and phosphate ($phosphate_{vessel}$) concentration in the chemostats, C, N, and P cell quotas, total particulate organic carbon, nitrogen, and phosphorus and associated ratios. (Note that some cell count data are missing due to technical issues).

Figure S3. Temporal changes in carbon cell quota (Q_C) and forward scatter (FSC) measured using flow cytometry in all 16 chemostats with different nutrient supply ratios (A – P). (Q) This illustrates the overall comparison between Q_C and FSC across all chemostats (red dots). The inserted statistics represent Spearman correlations between the variables.

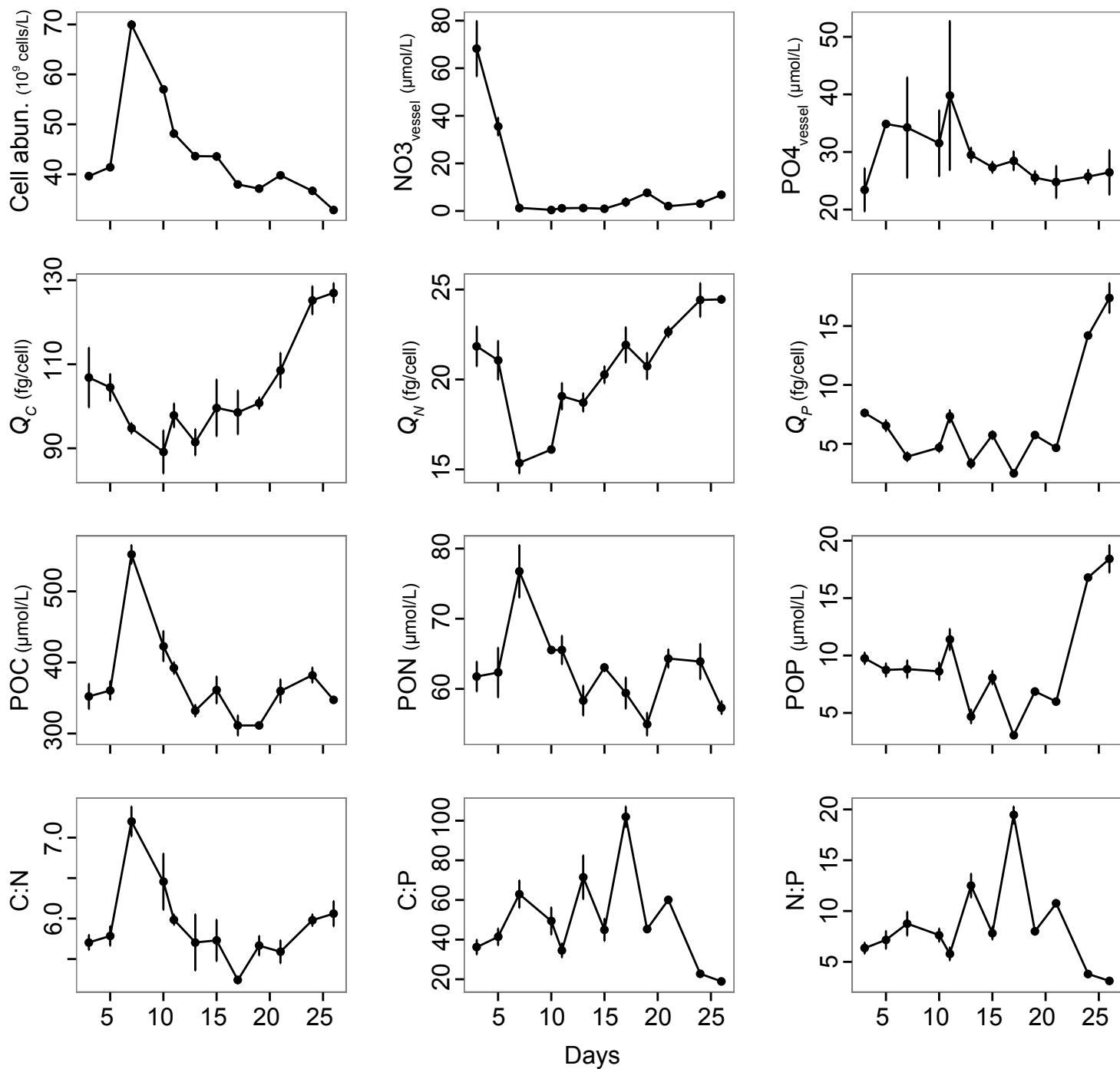


$N:P_{supply}$

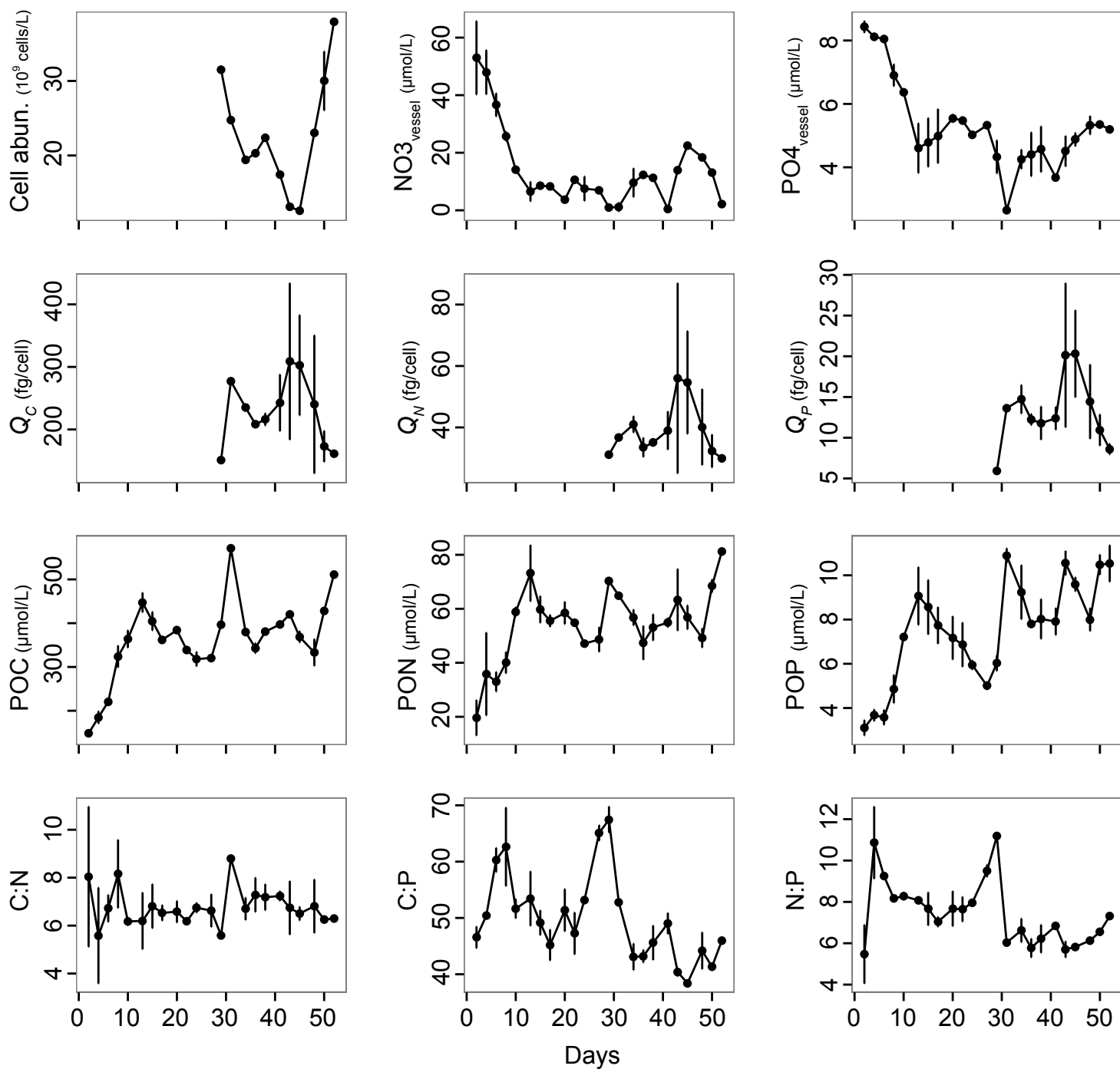




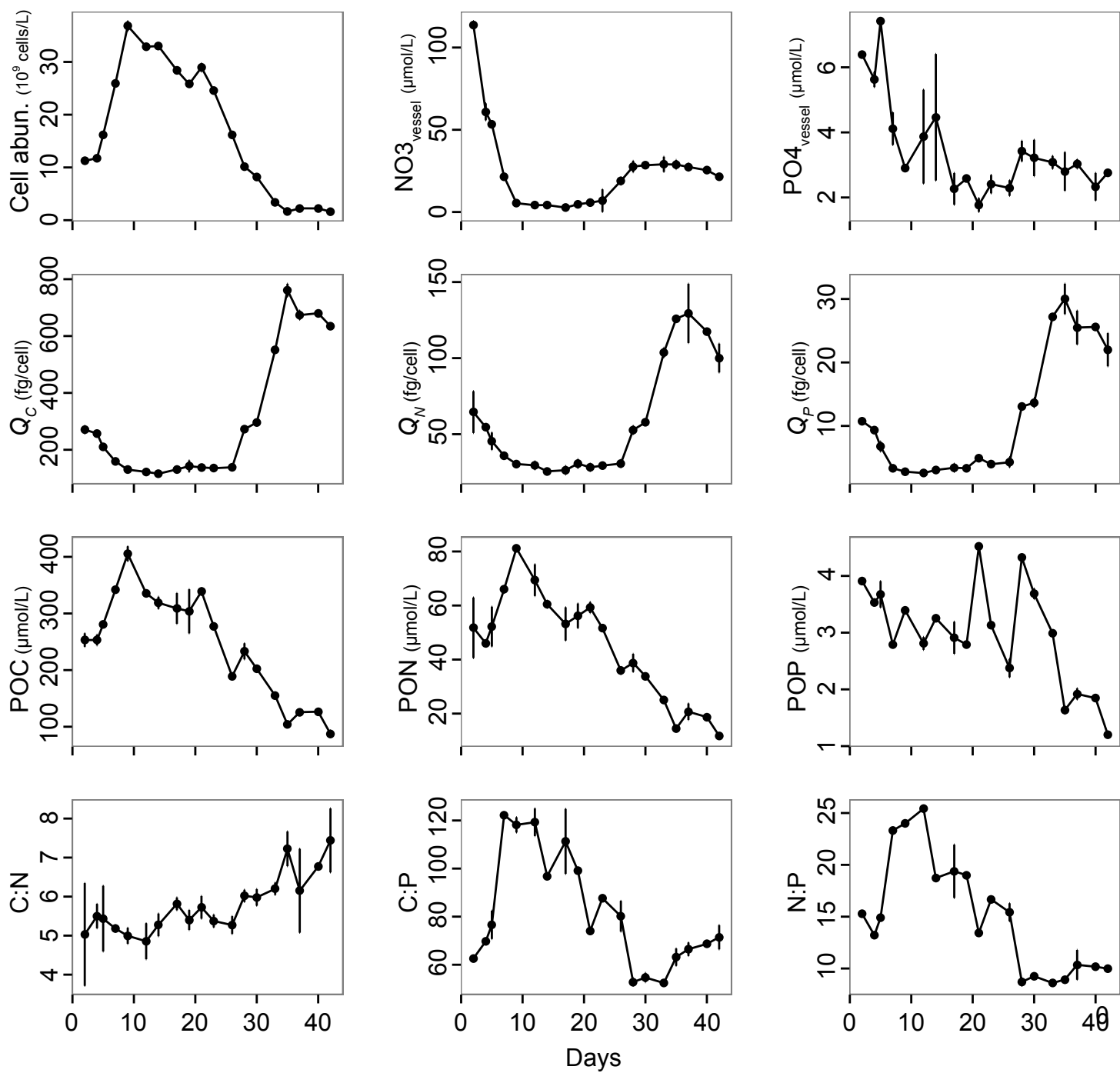
$N:P_{supply}=1$



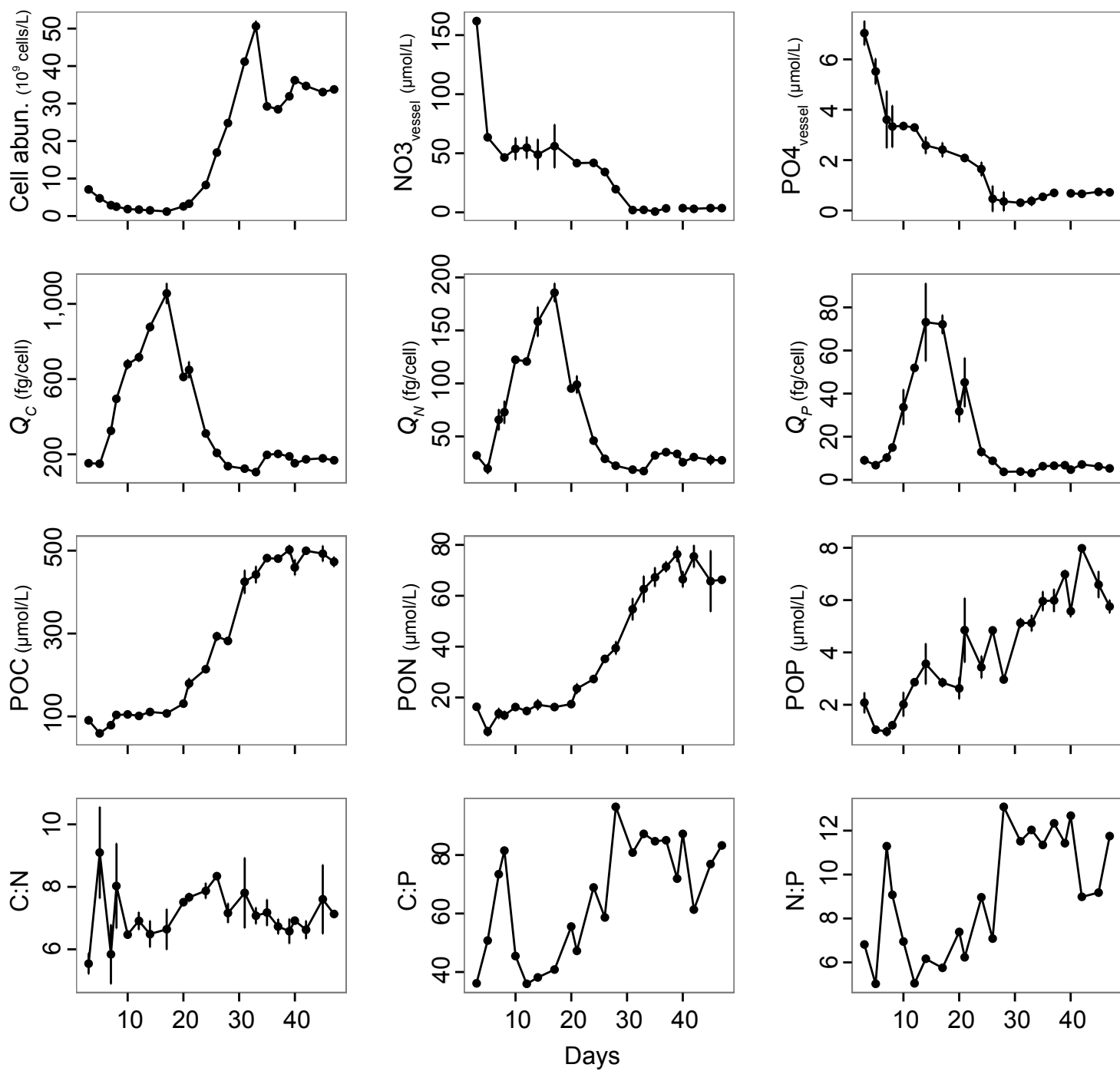
$N:P_{supply}=3$



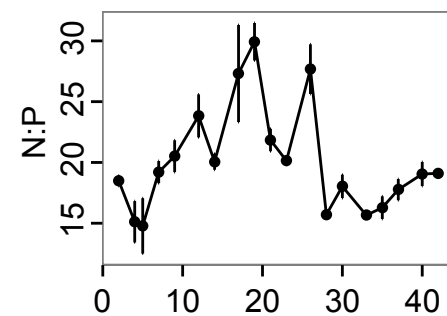
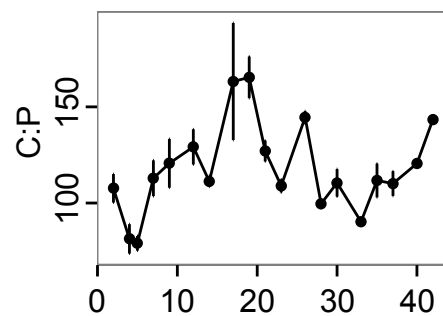
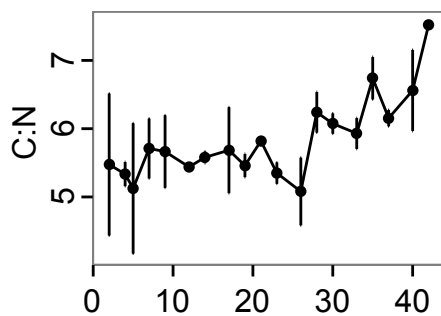
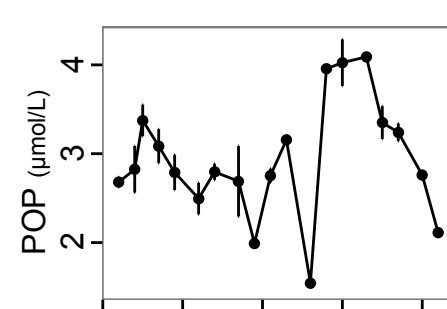
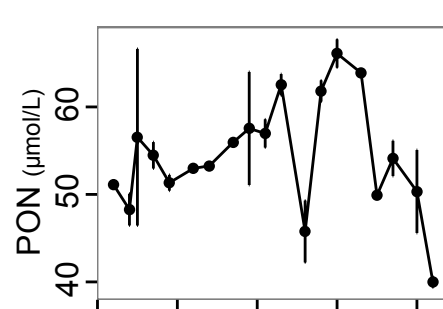
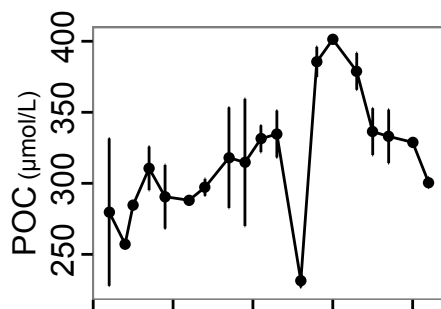
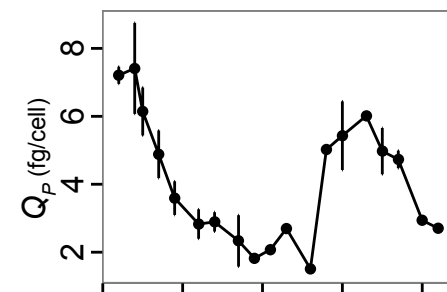
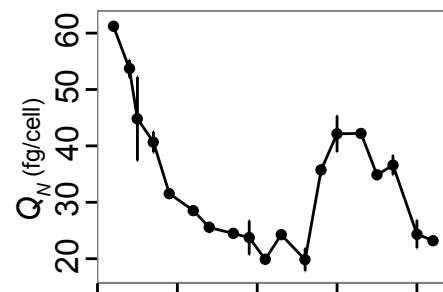
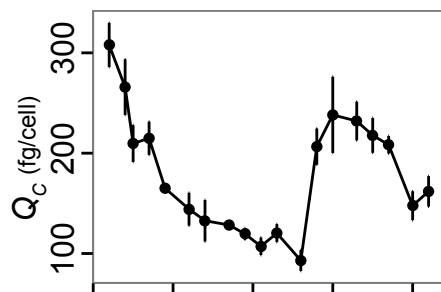
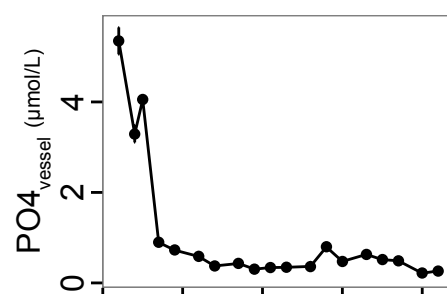
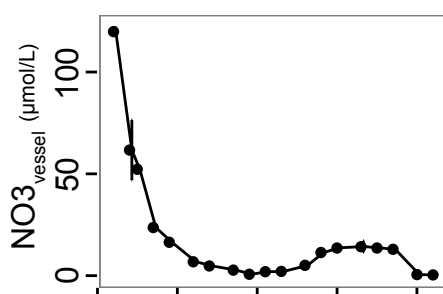
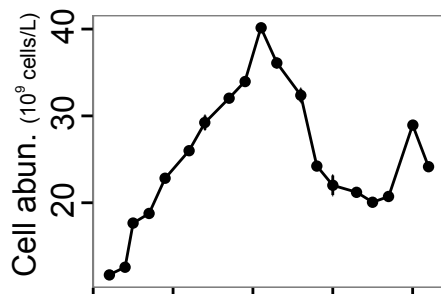
$N:P_{supply} = 5$



$N:P_{supply}=7$

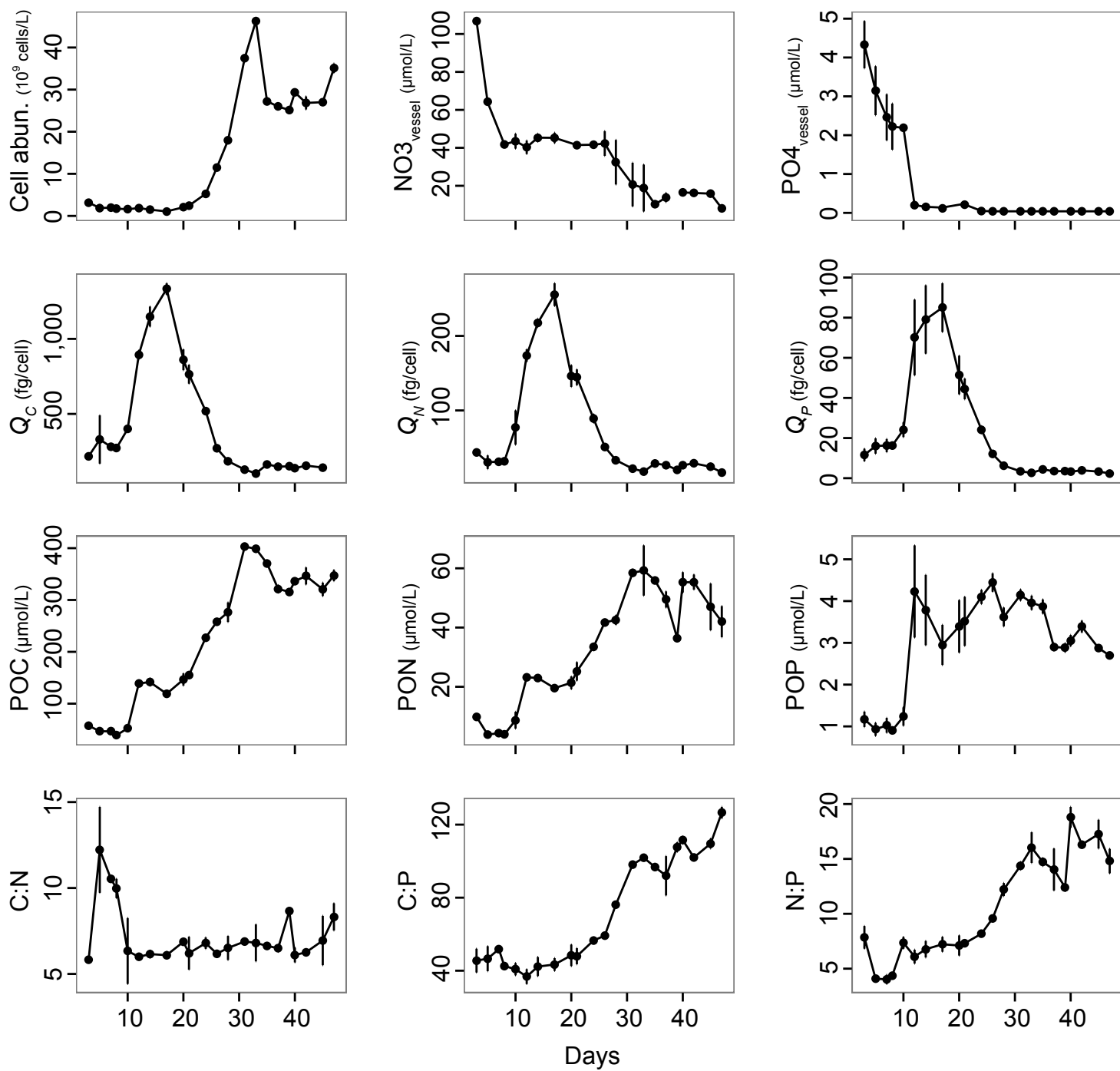


$N:P_{supply}=10$

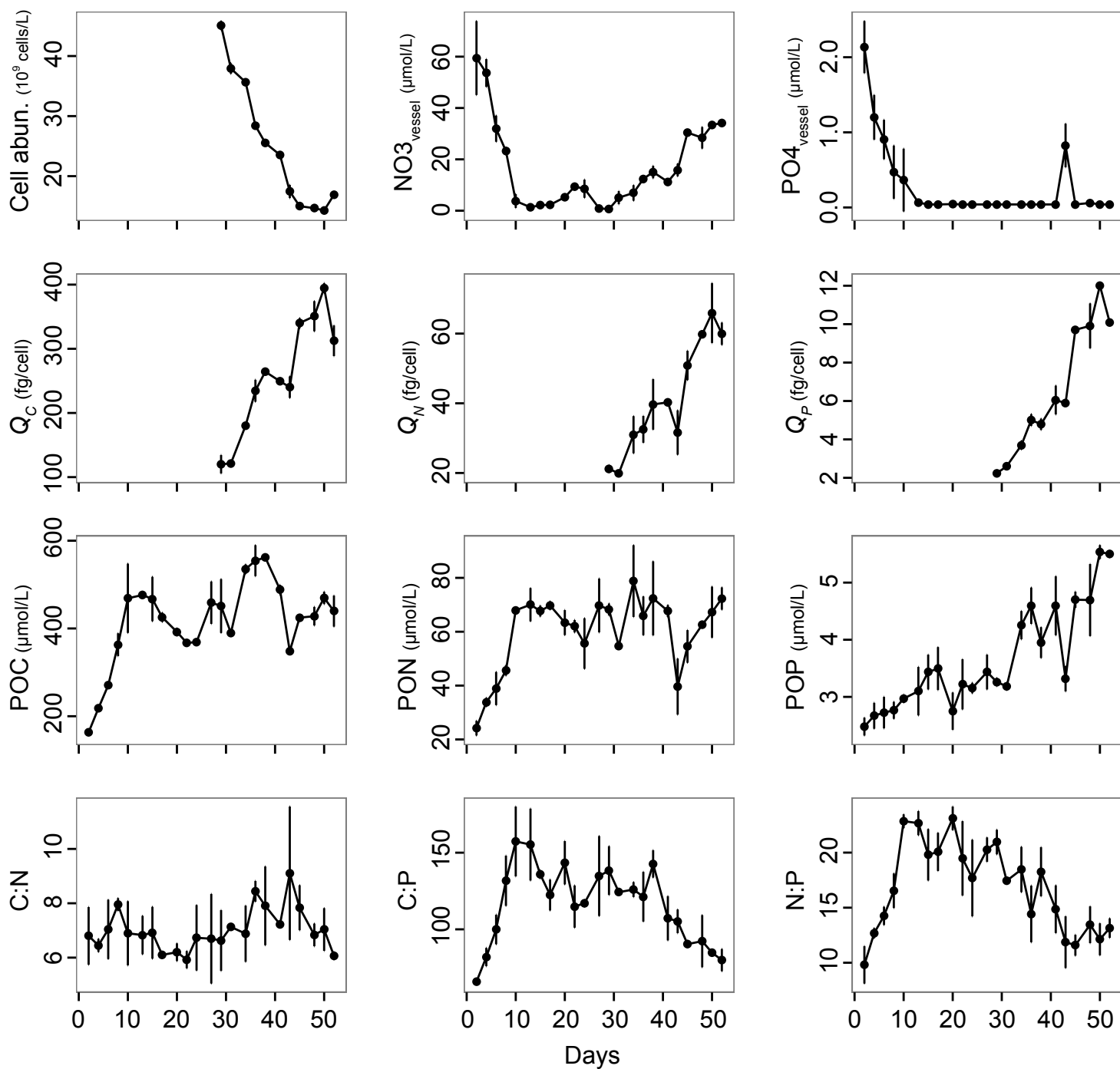


Days

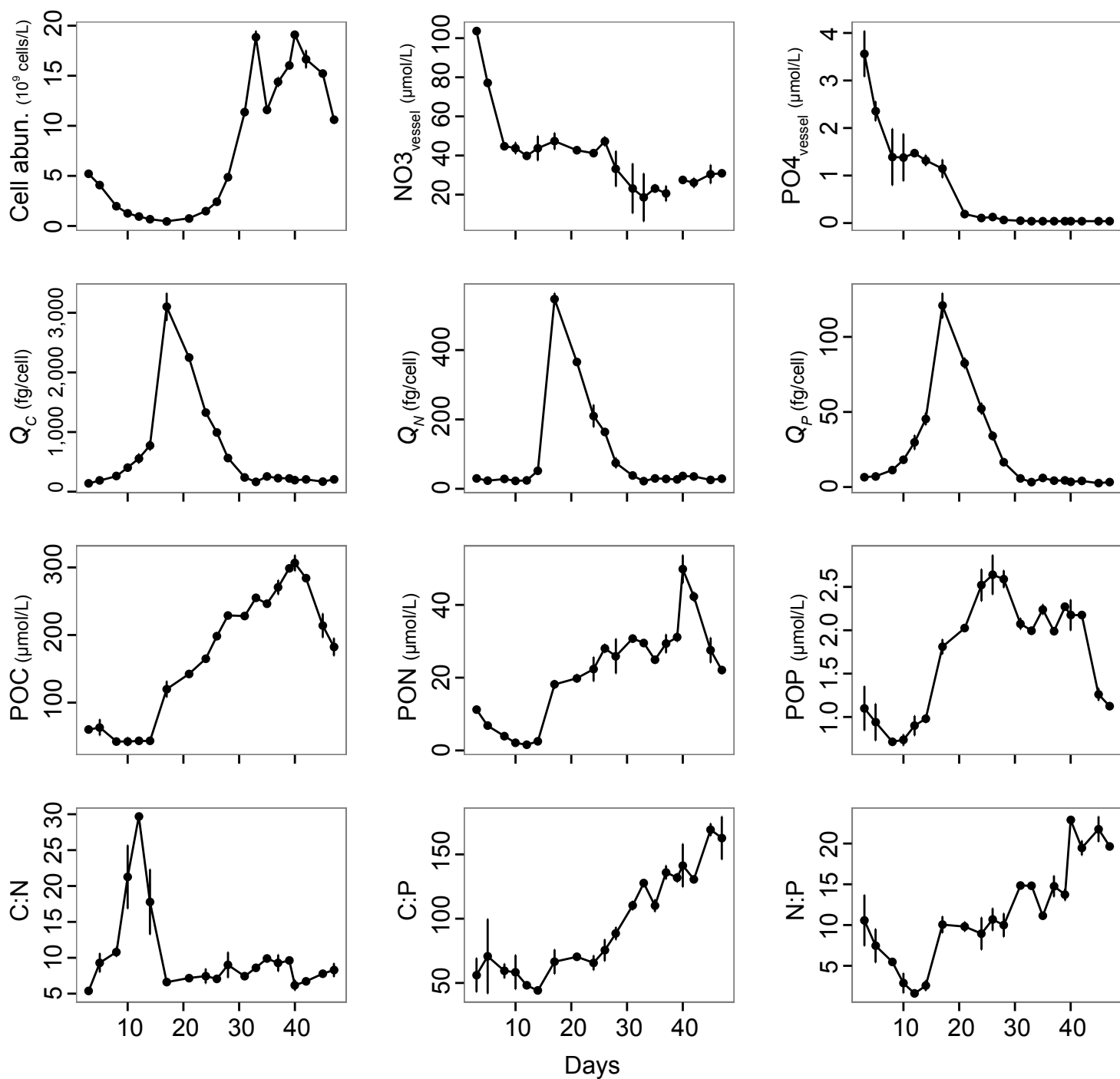
$N:P_{supply} = 12$



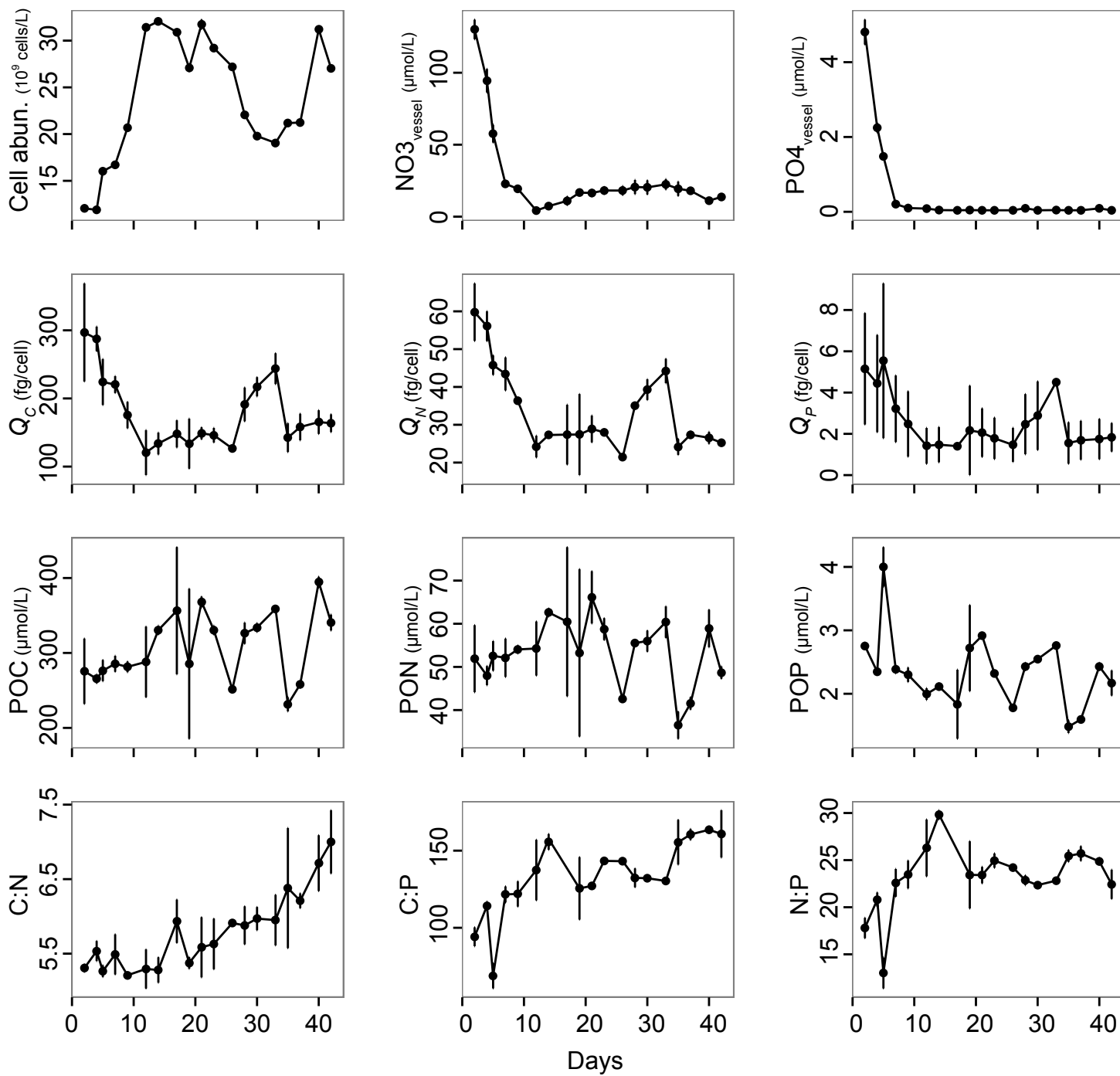
$N:P_{supply} = 15$



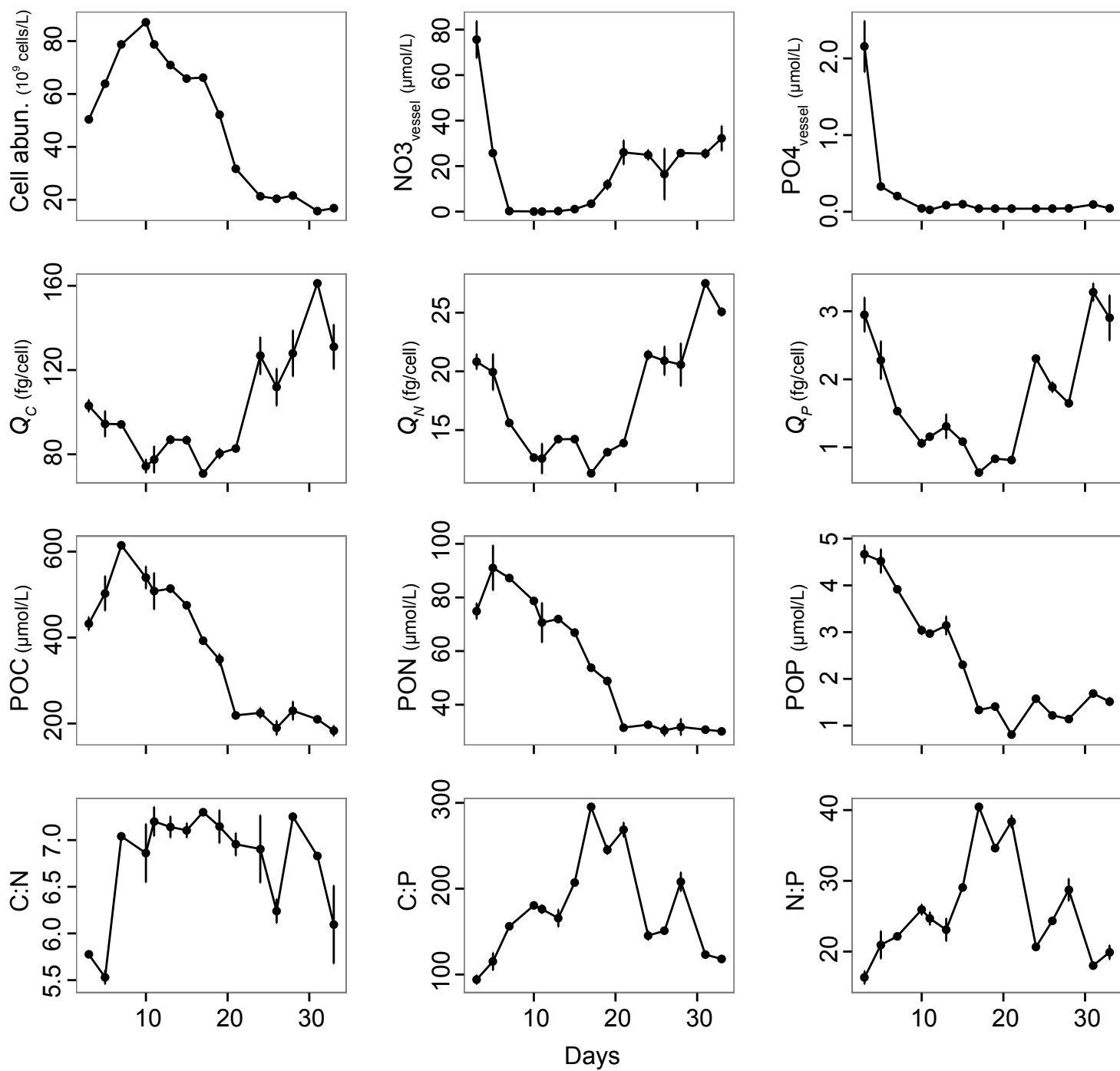
$N:P_{supply}=18$



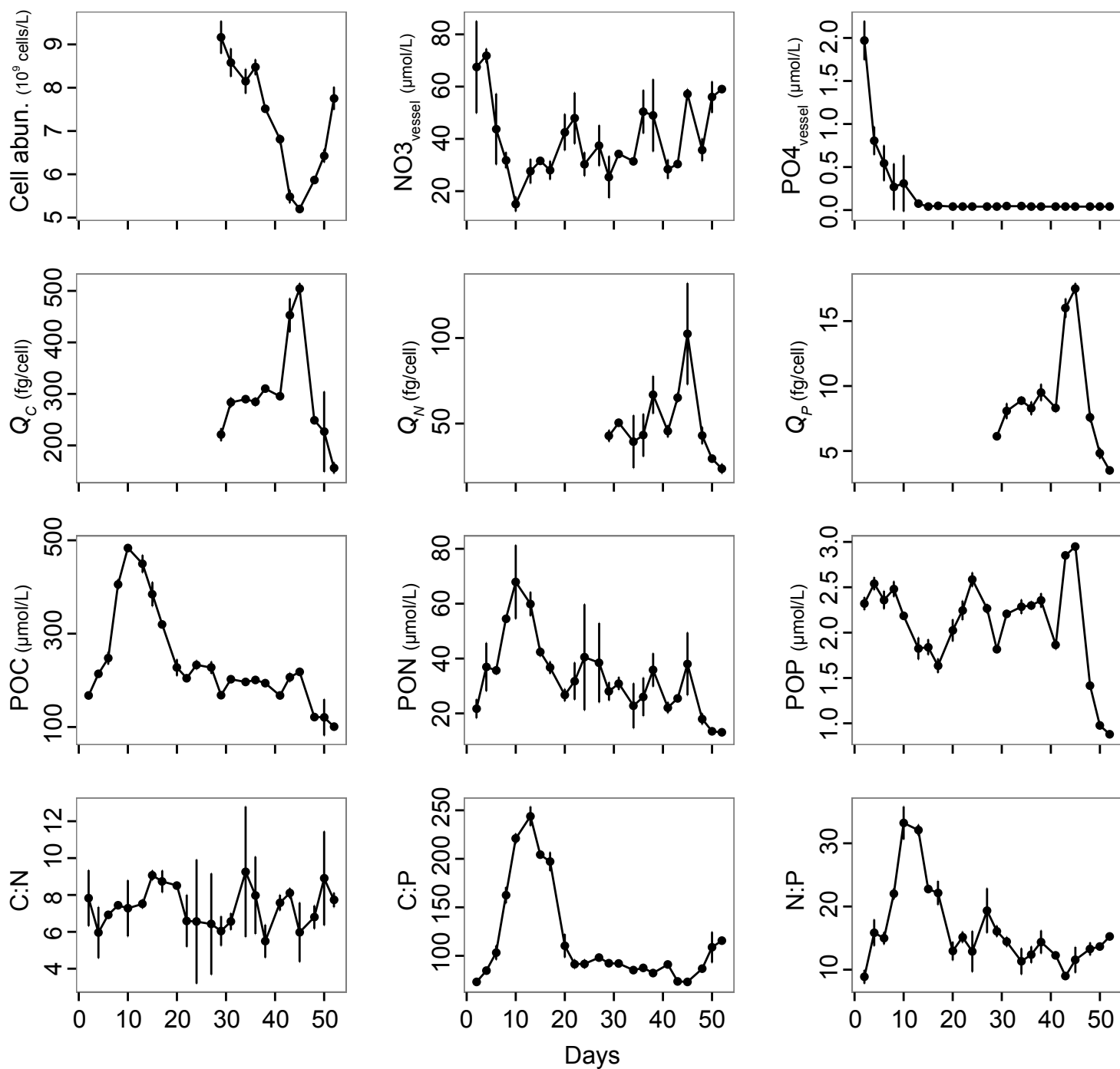
$N:P_{supply}=20$



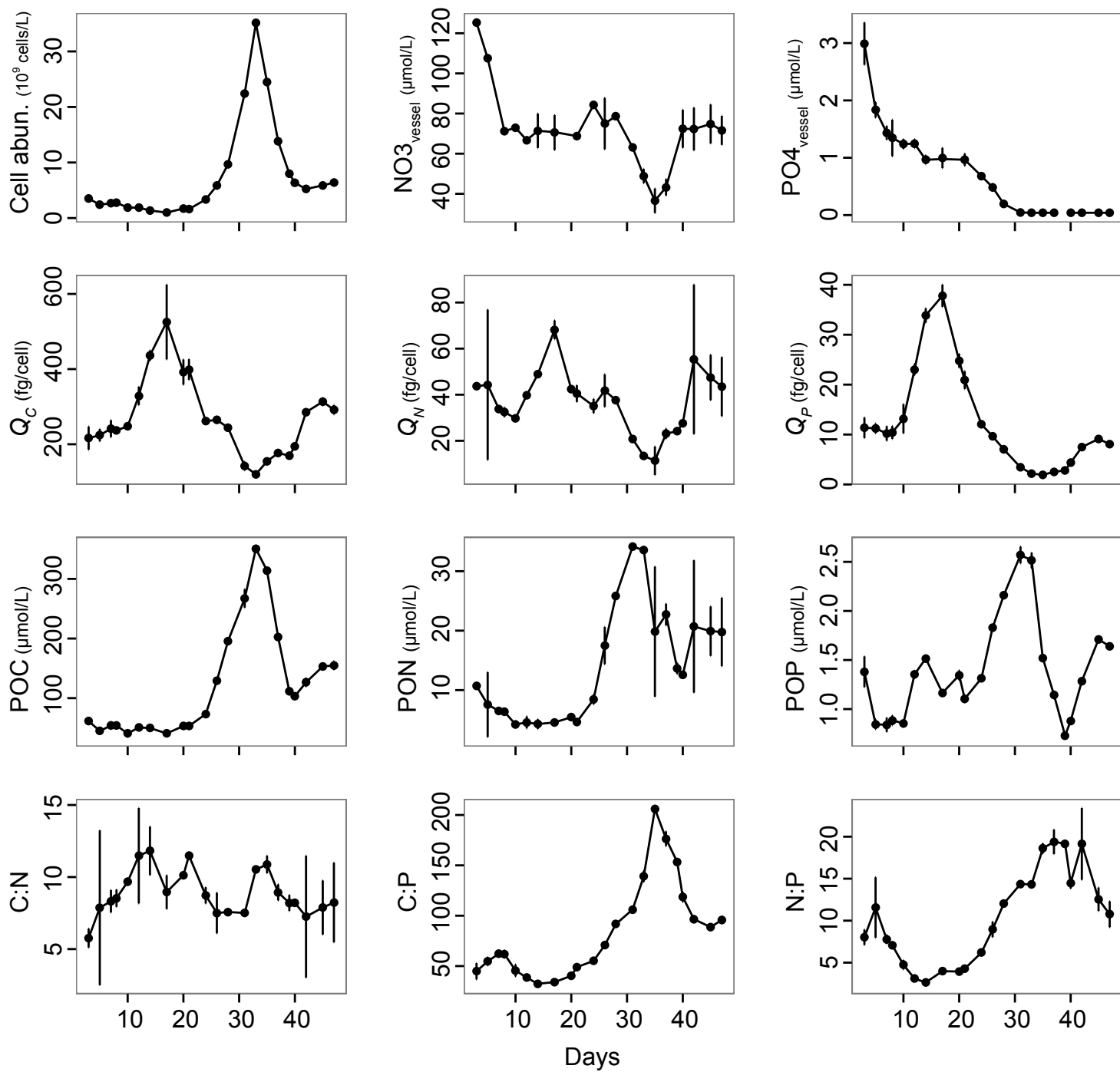
$N:P_{supply}=22$



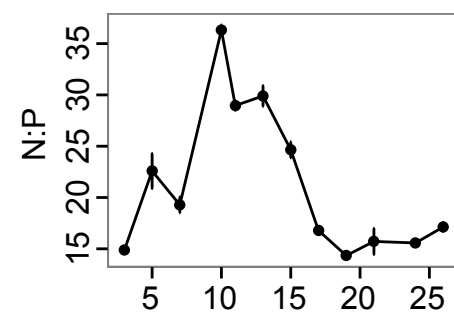
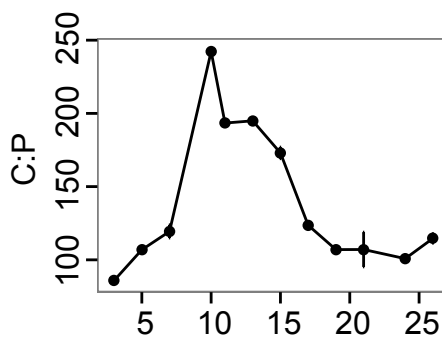
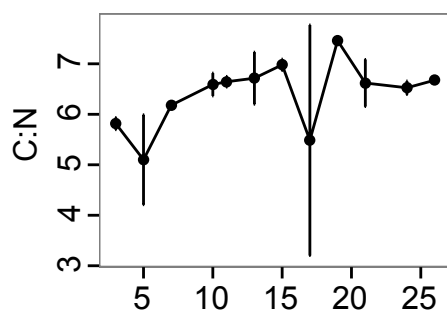
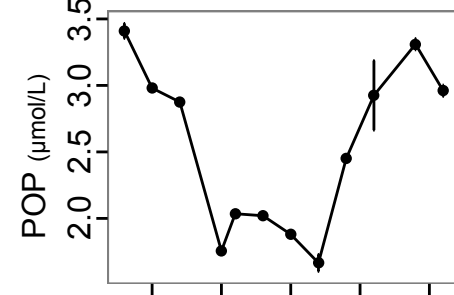
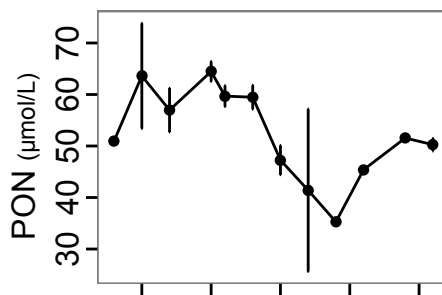
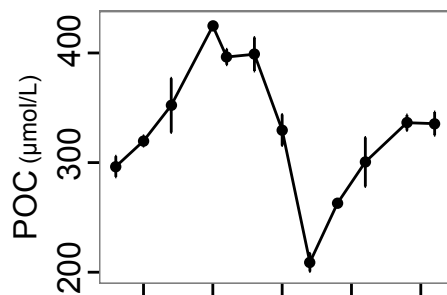
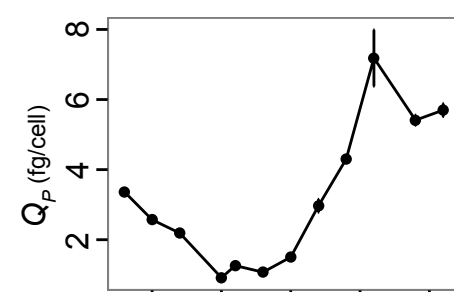
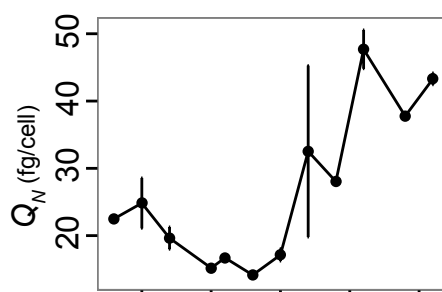
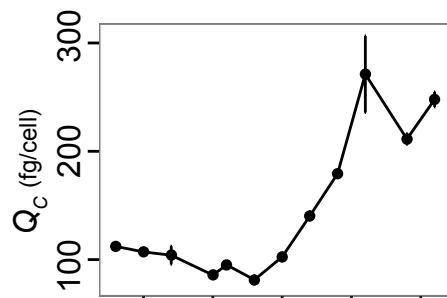
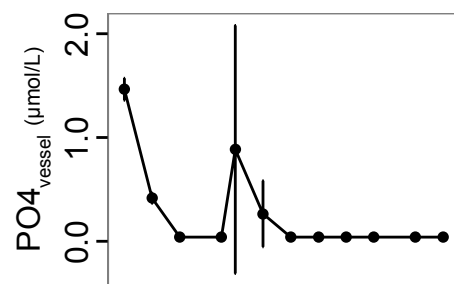
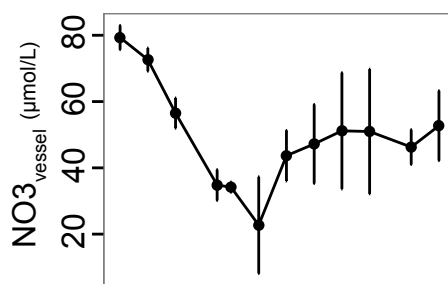
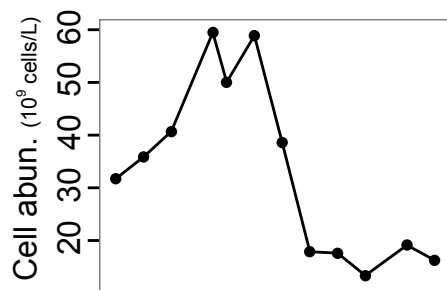
$N:P_{supply}=28$



$N:P_{supply}=35$

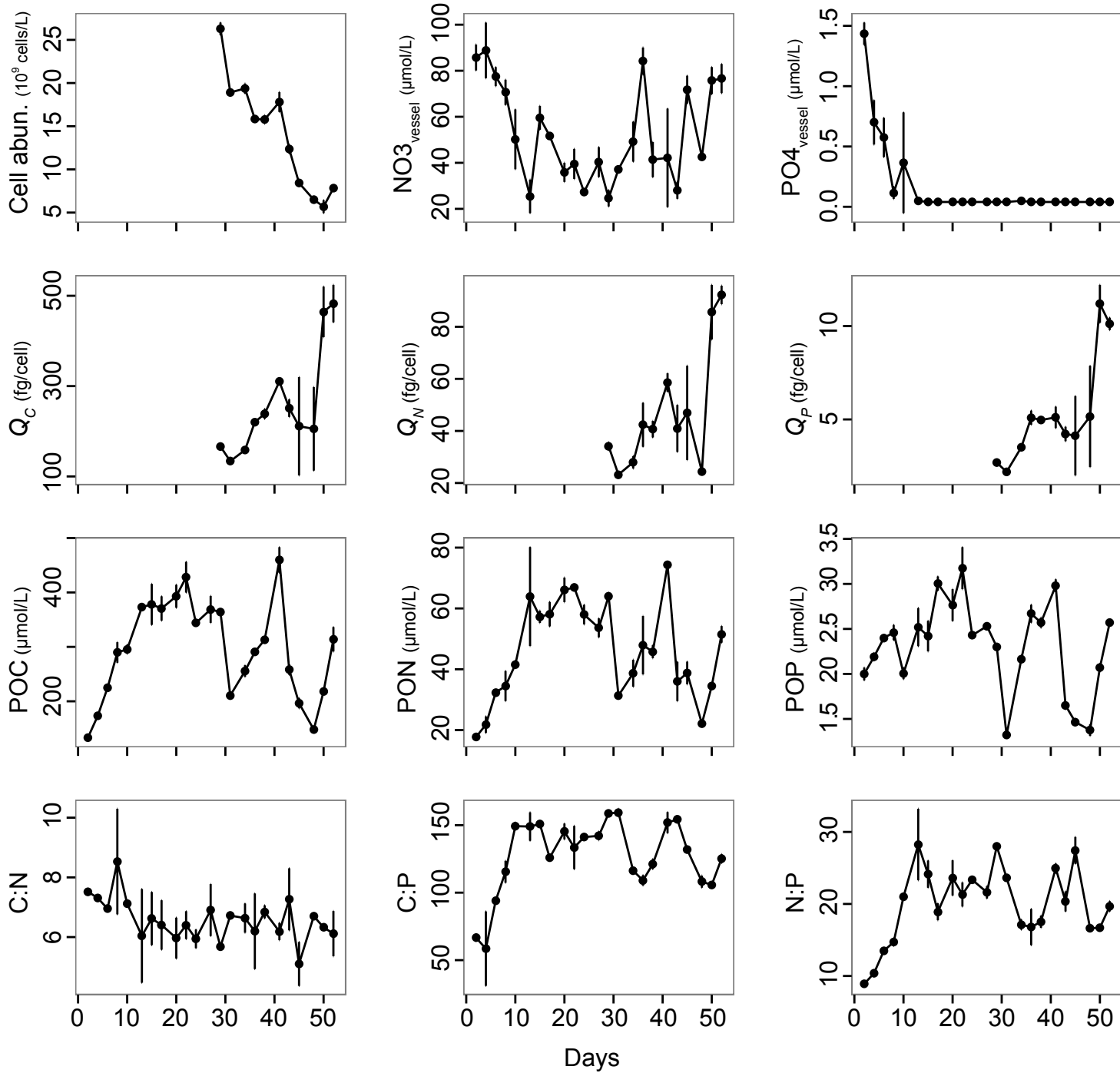


$N:P_{supply} = 38$



Days

$N:P_{supply} = 42$



$N:P_{supply}=50$

